Eur. Phys. J. E (2020) **43**: 54
DOI 10.1140/epje/i2020-11978-3

THE EUROPEAN PHYSICAL JOURNAL E

Regular Article

Charge regulation of a surface immersed in an electrolyte solution

P. Acharya and A.W.C. Lau[a]

Department of Physics, Florida Atlantic University, Boca Raton, FL 33431, USA

Received 14 May 2020 and Received in final form 6 July 2020
Published online: 14 August 2020

Abstract. In this paper, we investigate theoretically a model of charge regulation of a single charged planar surface immersed in an aqueous electrolyte solution. Assuming that the adsorbed ions are mobile in the charged plane, we formulate a field theory of charge regulation where the numbers of adsorbed ions can be determined consistently by equating the chemical potentials of the adsorbed ions to that of the ions in the bulk. We analyze the mean-field treatment of the model for electrolyte of arbitrary valences, and then beyond, where correlation effects are systematically taken into account in a loop expansion. In particular, we compute exactly various one-loop quantities, including electrostatic potentials, ion distributions, and chemical potentials, not only for symmetric $(1,1)$ electrolyte but also for asymmetric $(2,1)$ electrolyte, and make use of these quantities to address charge regulation at the one-loop level. We find that correlation effects give rise to various phase transitions in the adsorption of ions, and present phase diagrams for $(1,1)$ and $(2,1)$ electrolytes, whose distinct behaviors suggest that charge regulation, at the one-loop level, is no longer universal but depends crucially on the valency of the ions.

1 Introduction

Electrostatic interaction plays a crucial role in many physical processes in soft matter and biological systems that involve charged surfaces and ions in aqueous solutions [1–4]. The standard quantitative approach to study charged systems, in general, and charged surfaces, in particular, is the Poisson-Boltzmann (PB) theory, which is useful in evaluating the electrostatic potential, the ion distributions, and the electrostatic free energy, and provides an accurate description when the surface charge density and salt concentration are sufficiently low [3]. However, the PB theory fails spectacularly for systems that contain highly charged surfaces or the multivalent salts [5–7]. In these cases, the correlation effects, which the PB theory neglects, become important [8–12]. For example, the PB theory cannot explain experimentally observed phenomena (attributed to correlation effects) such as charge reversal [5, 7, 13] and like-charge attraction [14–18].

Moreover, many experiments [19–24] provide evidence for the fact that the counterion distribution, though it follows the functional form of the Gouy-Chapman solution [25,26], must be fitted with an effective surface charge density that is less than the original one. This deviation from the PB theory is attributed to the commonly used boundary conditions at the charged surface, known as constant charge boundary condition and constant potential boundary condition. Therefore, a third boundary condition, known as charge regulation boundary condition, has been introduced [27–30]. In a nutshell, charge regulation takes into account of processes that promote ion adsorption (either counterions, co-ions, or both) onto the surface, thereby renormalizing its surface charge density. One mechanism for counterion adsorption may be due to the Coulomb interaction itself. Since the counterions and surface charge are oppositely charged, bindings of the counterions to the surface can obviously occur and must be accounted for. Secondly, ion adsorption may be non-electrostatic in nature, such as chemical affinity between the ions and the charged surface, and short-ranged attraction such as van der Waals interaction or specific binding between the ions and the charged surface [31]. It is clear that neither of the boundary conditions above describes a variable surface charge that is regulated by these physical mechanisms.

The canonical model for charge regulation is proposed by Ninham and Parsegian (NP) [27], who extend the classical Langmuir model of adsorption of neutral particles to the case of ions onto a surface [32]. In a similar spirit of the Langmuir model, the NP charge regulation model assumes that the ions are adsorbed onto a discrete lattice (with exclusion), and additionally, it asserts

[a] e-mail: alau@fau.edu

that the ion concentration at the surface must be equal to the adsorbent concentration given by the Langmuir isotherm [32]. Therefore, the derivative of the electrostatic potential at the surface is related to a *renormalized* surface charge density, which leads to a non-linear charge regulation boundary condition. The NP charge regulation model has been extensively studied to address different phenomena [28,29,33–35], and in particular, it may give a viable interpretation for the discrepancy between the pressure (between similarly charged surfaces) predicted by the PB theory and that measured by atomic force microscopy experiments [21,23,24]. For example, Montes *et al.* [21] have measured the force between two charged surfaces across aqueous salt solutions containing ions of various valences, and their data show the necessity for charge regulation, especially for systems containing higher valence counterions, suggesting that Coulomb interaction may be one of physical mechanisms for charge regulation.

Despite its popularity, there is a few unsettling points that render the approximations made in the NP model questionable. First of all, the adsorbed ions and the surface charge density are not treated on the same footing [30]. In reality, all surface charges are discrete, but in the spirit of coarse-graining and mean-field nature of the PB theory, it may still be a good approximation to treat surface density as uniform. However, in the NP model, the original surface charge is treated as uniform, whereas the adsorbed ions are treated manifestly as discrete, since they are confined to the adsorbing sites on the lattice. But, treating the surface charges differently from those adsorbed may not have been a consistent coarse-grained physical picture, as pointed out in ref. [30]. Secondly, it is not immediately transparent that the boundary condition in the NP model follows from any physical principle, such as equating the chemical potentials or minimizing the free energy. More importantly, the NP charge regulation model is, at its heart, a mean-field theory, since it is based on the PB equation. And as it is so formulated, it is not immediately clear how to generalize the NP model to include correlation effects that are expected to be important for systems containing highly charged surfaces or multivalent salts [36–38].

In this paper, we propose and theoretically explore a model of charge regulation of a single uniformly charged planar surface immersed in an aqueous electrolyte solution. To model charge regulation consistently, we must have an appropriate model for ion adsorption, and a powerful framework to calculate consistently the effects of ion adsorption on the electrostatics of the system and vice versa. First, there are, in general, two kinds of model for particle adsorption —the Langmuir model [32,39,40], where particles are adsorbed onto the sites of a discrete 2D lattice with particles exclusion, and the Fowler-Guggenheim model [41], where the adsorbed particles form a 2D mobile surface layer, within which the adsorbed particles are free to move laterally. Since the charged surface is assumed to be uniformly charged, we opt for the Fowler-Guggenheim model. Secondly, to consistently calculate various electrostatic quantities (*e.g.*, electrostatic potential, ion distributions, adsorbed ion surface density, etc.), we formulate a field theory of charge regulation in which 1) free ions and adsorbed ions are treated on the same footing, consistent with the Fowler-Guggenheim model, 2) non-electrostatic bindings of ions to the surface can also be included, and 3) the adsorbed ion surface densities are determined by equating the chemical potentials of the adsorbed ions to that of the ions in the bulk.

More importantly, our framework allows us to investigate charge regulation not only at the mean-field level, but also beyond, where correlation effects are taken into account systematically via a loop expansion [8–12,36–38]. In particular, we derive a set of coupled non-linear equations (see eq. (32)), valid for arbitrary valences of the ions, from which the surface densities of the adsorbed ions can be determined self-consistently at the one-loop level. Furthermore, we explicitly analyze the model (at the one-loop level), not only for symmetric $(1,1)$ electrolyte but also for asymmetric $(2,1)$ electrolyte, thus allowing us to address the role of the valency of ions in charge regulation. Although our loop expansion is similar in spirit to those considered in the literature [9–12,36–38], our methods of exact evaluation of one-loop quantities may be generalized to study correlation effects in other problems in electrostatics. Indeed, to the best of our knowledge, it is for the first time that all the important one-loop quantities have been explicitly worked out for the exotic case of $(2,1)$ electrolyte [42].

Here is a summary of our major findings. At the mean-field level, we find, as expected, that 1) the number of adsorbed ions increases as the bare charge increases, 2) and as the salt concentration increases, for all valences; 3) the higher the valences, the more adsorbed ions there are, and 4) the coverage increases linearly with the pressure. The latter behavior indicates that at the mean-field level, ions are treated as an ideal gas. When correlation effects are taken into account at the one-loop level, the physics of charge regulation is drastically altered. We find that 5) the adsorption displays cooperative behaviors for high temperatures and low salt concentrations, 6) the adsorption displays various phase transitions (first-order and second-order) for low temperatures and high salt concentrations, and 7) the topologies of the phase diagrams for $(1,1)$ and $(2,1)$ electrolytes are quite distinct, suggesting that the physics of charge regulation is no longer universal but depends critically on the valency of the ions. In particular, we observe only for $(2,1)$ electrolyte that 8) charge regulation leads to charge reversal, and 9) the absorption exhibits reentrant behaviors.

The paper is organized as follows. In sect. 2, we present our model of charge regulation in detail, formulate it as a field theory, and use the latter to obtain consistently the equilibrium absorbed ion densities at the surface, first at the mean-field level and then at the one-loop level. We accomplish this in a few stages. First, we express the grand partition function for a system of ions (counterions and co-ions) in the presence a charged plane as a field theory in sect. 2.1. We then perform, in sect. 2.2, a loop expansion on the action functional, identify the mean-field approximation as the saddle point of the action, and obtain the absorbed ion densities at that level. In that section, we also

introduce an important parameter, which we will call the charge regulation parameter, that measures the extent to which the charged surface has been neutralized due to the adsorption of its counterions and co-ions. In sect. 2.3, we go beyond the mean-field approximation and obtain the one-loop chemical potentials of the ions, through an analysis of the Green's function (self-energy), one-loop corrections to the electrostatic potential, and one-loop ion distributions. In sect. 2.4, we derive exact expressions for the absorbed ion densities at one loop by equating the one-loop chemical potentials of the free ions and absorbed ions, valid for arbitrary p, see eq. (32). This is the central result of this paper, and the rest of the paper presents the predictions from this result.

In sect. 3, we explore the physics of charge regulation at the mean-field level. We first study the exact solutions to the PB equation for $p = 1$ and 2 with the charge regulation boundary condition imposed, and show how the charge regulation parameter varies with system parameters such as surface charge and salt concentration. We then present the absorption isotherms, defined as the coverage, proportional to the total number of ions absorbed as a function of pressure, for arbitrary p, and show that the coverage varies linearly with the pressure in the bulk. In sect. 4, we first discuss qualitatively the physics of ion adsorption at one loop and argue that correlation effects give rise to an effective binding energy that leads to phase transitions for the ion adsorptions under the right condition. We then present the phase diagram for $(1, 1)$ symmetric electrolyte in sect. 4.1 and for $(2, 1)$ asymmetric electrolyte in sect. 4.2 and discuss the behavior of the charge regulation parameter as a function of the surface charge in different parts of the phase diagram.

We relegate most of the mathematical details to the appendices. In appendix A.1, we discuss and obtain an explicit expression for the Green's function, a quantity that is the cornerstone of the one-loop calculation. In appendix A.2, we explicitly solve for the one-loop corrections to the electrostatic potential and discuss its behavior. In appendix A.3, we compute the one-loop Helmholtz free energy, which is needed to construct the phase diagrams. Lastly, in appendix B, we list those long mathematical expressions that may have been too distracting to be placed in the main text.

2 Field-theoretical formulation of charge regulation

In this section, we develop a field-theoretical formulation for charge regulation of a charged surface immersed in an aqueous solution with a uniform dielectric constant ϵ. Unlike the commonly used model of Langmuir [39, 40], where the adsorbed particles are bind to particular sites on the surface, our model is similar in spirit to the model of Fowler and Guggenheim [41], where the adsorbed particles (ions in our case) are confined laterally but are otherwise free to move parallel to the planar surface. This allows us to treat the adsorbed ions and the free ions (those ions that are not adsorbed) on the same footing and formulate a consistent theory, using which important thermodynamic quantities associated with this system can be computed. In particular, our framework allows us to calculate consistently the chemical potentials for both the adsorbed ions and the free ions. They are the crucial ingredients for our model of charge regulation because at equilibrium, the chemical potentials for the free and the adsorbed ions must be equal [41]. This equilibrium condition yields a pair of non-linear equations (see eq. (32)) from which the number densities of the adsorbed ions can be obtained, thus allowing us to predict the adsorption isotherms, which can be measured experimentally, under various conditions.

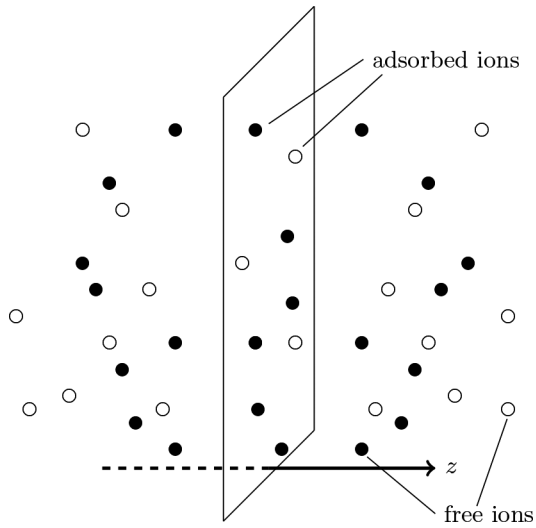

Fig. 1. A single negatively charged plane in an electrolyte solution, where the counterions (filled circles) of valence Z_+ and the co-ions (open circles) of valence Z_- are distributed on both sides of the plane, and a fraction of them adsorbed onto it. In equilibrium, the number densities of the adsorbed ions are determined by eq. (13) at the mean-field level and by eq. (32) at the one-loop level, where correlation effects are taken into account.

2.1 Grand partition function for a charged surface with adsorbed and free ions

Figure 1 shows a schematic picture of our system, which consists of N_+ point-like particles of charge Z_+e and N_- point-like particles of charge $-Z_-e$, where e is the proton charge. They are distributed on both sides of a single uniformly charged planar surface with a negative surface charge density $\sigma(\mathbf{x}) = -en_f(\mathbf{x}) = -en_0\delta(z)$ (see footnote [1]). In addition, to allow for charge regulation, we assume that N_{a+} point-like particles of charge Z_+e and N_{a-} point-like particles of charge $-Z_-e$ are adsorbed onto the surface with respective binding energies ε_+ and ε_- (in units of k_BT, where k_B is the Boltzmann constant, T is

[1] Without the loss of generality, we assume that the surface is negatively charged.

the temperature). As we will see below, $N_{a\pm}$ will be determined from the equilibrium condition that the chemical potentials for the absorbed ions and free ions be equal.

Assuming that the particles interact only through the Coulomb potential, we can write the total energy of the system as

$$\begin{aligned}\beta E_{N_\pm,\,N_{a\pm}} = &-N_{a+}\,\varepsilon_+ - N_{a-}\,\varepsilon_- - (N_+ + N_{a+})\,V_0^+ \\ &- (N_- + N_{a-})\,V_0^- - \int \mathrm{d}^3\mathbf{x}\,\hat{\rho}(\mathbf{x})\phi(\mathbf{x}) \\ &+\frac{l_B}{2}\int \mathrm{d}^3\mathbf{x}\int \mathrm{d}^3\mathbf{x}'\,\frac{\hat{\rho}(\mathbf{x})\hat{\rho}(\mathbf{x}')}{|\mathbf{x}-\mathbf{x}'|}\,, \end{aligned} \tag{1}$$

where the first two terms represent the non-electrostatic binding energy of the ions, $\beta \equiv k_BT$, $l_B \equiv e^2/(\epsilon k_BT) \approx 7\,\text{Å}$ is the Bjerrum length in water at room temperature, $\phi(\mathbf{x}) \equiv l_B \int \mathrm{d}^3\mathbf{x}' \frac{n_f(\mathbf{x}')}{|\mathbf{x}-\mathbf{x}'|}$ is the external potential due to the presence of the charged surface, $V_0^\pm \equiv \frac{4\pi Z_\pm^2 l_B}{2}\int \frac{\mathrm{d}^2\mathbf{q}}{(2\pi)^2}\frac{1}{2q}$ are the bare (infinite) self-energies of the free ions and the adsorbed ions[2], and $\hat{\rho}(\mathbf{x})$ is the total charge density operator for the system, defined as

$$\begin{aligned}\hat{\rho}(\mathbf{x}) = &Z_+\sum_{i=1}^{N_+}\delta^{(3)}(\mathbf{x}-\mathbf{x}_i^+) + Z_+\delta(z)\sum_{i=1}^{N_{a+}}\delta^{(2)}(\mathbf{r}-\mathbf{r}_i^+) \\ &-Z_-\sum_{i=1}^{N_-}\delta^{(3)}(\mathbf{x}-\mathbf{x}_i^-) - Z_-\delta(z)\sum_{i=1}^{N_{a-}}\delta^{(2)}(\mathbf{r}-\mathbf{r}_i^-),\end{aligned}$$

where the first and third term represent, respectively, a set of N_+ positive and N_- negative charges located at $\mathbf{x}_i^+$ and $\mathbf{x}_i^-$, and the second and fourth term represent, respectively, a set of N_{a+} positive and N_{a-} negative adsorbed ions that are confined to $z=0$ and located at $\mathbf{r}_i^+$ and $\mathbf{r}_i^-$ in the plane.

The canonical partition function for this system is

$$\begin{aligned}Z_{N_\pm,\,N_{a\pm}}[\phi(\mathbf{x})] = &\frac{1}{N_+!}\left(\prod_{i=1}^{N_+}\int\frac{\mathrm{d}^3\mathbf{x}_i^+}{a_+^3}\right) \\ &\times\frac{1}{N_-!}\left(\prod_{i=1}^{N_-}\int\frac{\mathrm{d}^3\mathbf{x}_i^-}{a_-^3}\right)\frac{1}{N_{a+}!}\left(\prod_{i=1}^{N_{a+}}\int\frac{\mathrm{d}^2\mathbf{r}_i^+}{a_{c+}^2}\right) \\ &\times\frac{1}{N_{a-}!}\left(\prod_{i=1}^{N_{a-}}\int\frac{\mathrm{d}^2\mathbf{r}_i^-}{a_{c-}^2}\right)e^{-\beta E_{N_\pm,\,N_{a\pm}}},\end{aligned} \tag{2}$$

where $a_\pm$ are the ionic sizes of the positive and negative free ions, respectively, and $a_{c\pm}$ are the ionic sizes of the positive and negative adsorbed ions, respectively. Introducing the chemical potentials (in units of k_BT), $\mu_\pm$ and $\mu_{a\pm}$, for the free and the adsorbed ions (positive and negative), respectively, we can write, after performing the Hubbard-Stratonovitch transformation [43,44], the grand-canonical partition function as

$$\mathcal{Z}_{\mu_\pm,\,\mu_{a\pm}}[\phi(\mathbf{x})] = \mathcal{N}_0\int\mathcal{D}\,\psi(\mathbf{x})\,e^{-\mathcal{S}[\psi(\mathbf{x}),\phi(\mathbf{x})]}, \tag{3}$$

where $\psi(\mathbf{x})$ is the fluctuating field, $\mathcal{N}_0$ is the normalization constant, and $\mathcal{S}$ is the action functional

$$\begin{aligned}\mathcal{S} = \frac{1}{\ell_B}\int\mathrm{d}^3\mathbf{x}\,\Big\{&\frac{1}{2}\,\psi(\mathbf{x})[-\nabla_{\mathbf{x}}^2]\psi(\mathbf{x}) - \Lambda_+\,e^{p[\imath\psi(\mathbf{x})+Z\phi(\mathbf{x})]} \\ &-\Lambda_-\,e^{-[\imath\psi(\mathbf{x})+Z\phi(\mathbf{x})]} - \Lambda_{a+}e^{p[\imath\psi(\mathbf{x})+Z\phi(\mathbf{x})]}\delta(z) \\ &-\Lambda_{a-}e^{-[\imath\psi(\mathbf{x})+Z\phi(\mathbf{x})]}\delta(z)\Big\},\end{aligned} \tag{4}$$

where, for simplicity, we have assumed, without loss of generality, that $Z_+ \equiv pZ_- \equiv pZ$ and rescaled the field by $\psi \to Z\psi$. We have also defined the modified Bjerrum length by $\ell_B \equiv 4\pi Z^2 l_B$, and four important parameters by $\Lambda_\pm \equiv \ell_B[\exp(\mu_\pm + V_0^\pm)]/a_\pm^3$ and $\Lambda_{a\pm} \equiv \ell_B[\exp(\mu_{a\pm}+V_0^\pm+\varepsilon_\pm)]/a_{c\pm}^2$, which are related to chemical potentials of the free and the adsorbed ions, respectively; $\Lambda_\pm$ have the dimensions of $1/[\text{Length}]^2$, whereas $\Lambda_{a\pm}$ have the dimensions of $1/[\text{Length}]$, and they contain the infinite self-energy term $V_0^\pm$. We note that for $p=1$, our action functional, eq. (4), reduces to that of refs. [9–12], which consider the fluctuation contributions of monovalent ions to the surface tension.

The thermal average of a given physical quantity is generated by the grand-canonical partition function in eq. (3). For example, the distributions of the free ions are

$$\begin{aligned}\langle\hat{\rho}_\pm(\mathbf{x})\rangle_{\text{eq}} &= \left\langle\sum_{i=0}^{N_\pm}\delta(\mathbf{x}-\mathbf{x}_i^\pm)\right\rangle_{\text{eq}} \\ &= \frac{\Lambda_\pm}{\ell_B}\left\langle e^{\pm(Z_\pm/Z)[\imath\psi(\mathbf{x})+Z\phi(\mathbf{x})]}\right\rangle,\end{aligned} \tag{5}$$

where $\langle\mathcal{F}[\psi(\mathbf{x})]\rangle = \mathcal{Z}^{-1}_{\mu_\pm,\,\mu_{a\pm}}\int\mathcal{D}\,\psi(\mathbf{x})\,\mathcal{F}[\psi(\mathbf{x})]e^{-\mathcal{S}}$, for any functional $\mathcal{F}[\psi(\mathbf{x})]$. Note that $Z_+/Z = p$ and $Z_-/Z = 1$. Similarly, the distributions for the adsorbed ions are given by

$$\langle\hat{\rho}_{a\pm}(\mathbf{x})\rangle_{\text{eq}} = \frac{\Lambda_{a\pm}}{\ell_B}\left\langle e^{\pm(Z_\pm/Z)[\imath\psi(\mathbf{x})+Z\phi(\mathbf{x})]}\right\rangle\delta(z). \tag{6}$$

The charge neutrality condition in terms of these distributions is given by

$$\begin{aligned}\int\mathrm{d}^3\mathbf{x}\,\Big[&p\,\langle\hat{\rho}_+(\mathbf{x})\rangle_{\text{eq}} - \langle\hat{\rho}_-(\mathbf{x})\rangle_{\text{eq}} \\ &+p\,\langle\hat{\rho}_{a+}(\mathbf{x})\rangle_{\text{eq}} - \langle\hat{\rho}_{a-}(\mathbf{x})\rangle_{\text{eq}}\Big] = \frac{n_0\mathcal{A}}{Z}\,,\end{aligned} \tag{7}$$

where $\mathcal{A}$ is the area of the surface.

2.2 Loop expansion and the adsorbed ion surface densities at mean field

To investigate correlation effects on charge regulation systematically, we perform a loop expansion on the action

[2] The self-energy arises from the fact that the last integral in eq. (1) contains terms that are evaluated at $\mathbf{x}=\mathbf{x}'$. See ref. [8].

given by eq. (4) by generalizing the treatment for a similar system as done in ref. [8]. We identify the modified Bjerrum length ℓ_B as the expansion parameter and write the fluctuating field $\psi(\mathbf{x})$ as $\psi(\mathbf{x}) = \psi_0(\mathbf{x}) + \Delta\psi(\mathbf{x})$ and the parameters, $\Lambda_\pm$ and $\Lambda_{a\pm}$, as $\Lambda_\pm = \Lambda_\pm^{(0)} + \delta\Lambda_\pm$ and $\Lambda_{a\pm} = \Lambda_{a\pm}^{(0)} + \delta\Lambda_{a\pm}$, where $\Delta\psi(\mathbf{x})$ is of the order of $\sqrt{\ell_B}$ and $\delta\Lambda_{a\pm}$ and $\delta\Lambda_{a\pm}$ are of the order of ℓ_B. Expanding eq. (4) up to first order in ℓ_B, we find

$$\begin{aligned}\mathcal{S} = \mathcal{S}[\psi_0(\mathbf{x}), \phi(\mathbf{x})] \\ +\frac{1}{2}\int \mathrm{d}^3\mathbf{x}\int \mathrm{d}^3\mathbf{x}'\Delta\psi(\mathbf{x})K(\mathbf{x},\mathbf{x}')\Delta\psi(\mathbf{x}') \\ -\frac{1}{\ell_B}\int \mathrm{d}^3\mathbf{x}\left\{F(\mathbf{x})[\imath\Delta\psi(\mathbf{x})] - \frac{1}{3!}H(\mathbf{x})[\imath\Delta\psi(\mathbf{x})]^3\right\} \\ -\frac{1}{\ell_B}\int \mathrm{d}^3\mathbf{x}\left\{[\delta\Lambda_+ + \delta\Lambda_{a+}\delta(z)]\, e^{p[\imath\psi_0(\mathbf{x})+Z\phi(\mathbf{x})]}\right. \\ \left. + [\delta\Lambda_- + \delta\Lambda_{a-}\delta(z)]\, e^{-[\imath\psi_0(\mathbf{x})+Z\phi(\mathbf{x})]}\right\} + \mathcal{O}(\ell_B). \quad (8)\end{aligned}$$

Here, we have chosen $\psi_0(\mathbf{x})$ to satisfy

$$\begin{aligned}&\nabla^2_{\mathbf{x}}[\imath\psi_0(\mathbf{x})] - p\Lambda_+^{(0)}e^{p[\imath\psi_0(\mathbf{x})+Z\phi(\mathbf{x})]} + \Lambda_-^{(0)}e^{-[\imath\psi_0(\mathbf{x})+Z\phi(\mathbf{x})]} \\ &= \left\{p\Lambda_{a+}^{(0)}e^{p[\imath\psi_0(\mathbf{x})+Z\phi(\mathbf{x})]} - \Lambda_{a-}^{(0)}e^{-[\imath\psi_0(\mathbf{x})+Z\phi(\mathbf{x})]}\right\}\delta(z),\end{aligned} \quad (9)$$

so that the linear term proportional to $\Delta\psi(\mathbf{x})$ in the expansion of the action in eq. (8) vanishes identically. Equation (9) can be cast into the mean-field PB equation

$$\begin{aligned}&-\nabla^2\varphi_0(\mathbf{x}) + \frac{\kappa^2}{1+p}\left[e^{p\varphi_0(\mathbf{x})} - e^{-\varphi_0(\mathbf{x})}\right] = \\ &\frac{\ell_B}{Z}\left[n_0 - Z(pn_{a+} - n_{a-})\right]\delta(z),\end{aligned} \quad (10)$$

with a simple transformation

$$\varphi_0(\mathbf{x}) \equiv \imath\psi_0(\mathbf{x}) + Z\phi(\mathbf{x}) + \frac{1}{1+p}\ln\left[\frac{p\Lambda_+^{(0)}}{\Lambda_-^{(0)}}\right], \quad (11)$$

where $\varphi_0(\mathbf{x})$ may be interpreted physically as the mean-field electrostatic potential,

$$\kappa^2 \equiv (1+p)\left[p\Lambda_+^{(0)}\left(\Lambda_-^{(0)}\right)^p\right]^{1/(1+p)}, \quad (12)$$

is the inverse of the Debye screening length squared, and $n_{a\pm}$ are defined as

$$n_{a\pm} = \frac{\kappa^2}{(Z_\pm/Z)(1+p)\ell_B}\left(\frac{\Lambda_{a\pm}^{(0)}}{\Lambda_\pm^{(0)}}\right)e^{\pm(Z_\pm/Z)\varphi_0(0)}. \quad (13)$$

They have the obvious physical interpretation of the number densities of the positive and negative adsorbed ions, respectively. Indeed, it is easy to see from eq. (10) that one of the effects of the adsorbed ions is to renormalize the surface charge, $n_0 \to n_0 - Z(pn_{a+} - n_{a-})$. Note that because of the planar geometry, the mean-field solution $\varphi_0(\mathbf{x})$ depends only on z.

Going back to eq. (8), the operator $K(\mathbf{x},\mathbf{x}')$ and the two functions, $F(\mathbf{x})$ and $H(\mathbf{x})$, can be written, with the help of eqs. (11) and (13), as

$$\begin{aligned}K(\mathbf{x},\mathbf{x}') = \frac{1}{\ell_B}\left\{-\nabla^2_{\mathbf{x}} + \frac{\kappa^2}{1+p}\left[p\,e^{p\varphi_0(\mathbf{x})} + e^{-\varphi_0(\mathbf{x})}\right]\right. \\ \left. +\frac{2}{\lambda_D}\,\delta(z)\right\}\delta(\mathbf{x}-\mathbf{x}'),\end{aligned} \quad (14)$$

$$\begin{aligned}F(\mathbf{x}) = \frac{\kappa^2}{1+p}\left[\frac{\delta\Lambda_+}{\Lambda_+^{(0)}}\,e^{p\varphi_0(\mathbf{x})} - \frac{\delta\Lambda_-}{\Lambda_-^{(0)}}\,e^{-\varphi_0(\mathbf{x})}\right] \\ +\ell_B\left[pn_{a+}\frac{\delta\Lambda_{a+}}{\Lambda_{a+}^{(0)}} - n_{a-}\frac{\delta\Lambda_{a-}}{\Lambda_{a-}^{(0)}}\right]\delta(z),\end{aligned} \quad (15)$$

$$\begin{aligned}H(\mathbf{x}) = \frac{\kappa^2}{1+p}\left[p^2e^{p\varphi_0(\mathbf{x})} - e^{-\varphi_0(\mathbf{x})}\right] \\ +\ell_B\left(p^3n_{a+} - n_{a-}\right)\delta(z),\end{aligned} \quad (16)$$

where we have defined $2/\lambda_D \equiv \ell_B(p^2n_{a+} + n_{a-})$.

At the mean-field level, the equilibrium values for the number densities of the adsorbed ions, $n_{a\pm}$, can be obtained by i) setting $\Lambda_{a\pm}^{(0)}/\Lambda_\pm^{(0)} = e^{\varepsilon_\pm}(a_\pm^3/a_{c\pm}^2)$, which is equivalent to $\mu_{a\pm}^{(0)} = \mu_\pm^{(0)}$, and ii) evaluating the potential $\varphi_0(z)$ at the plate (at $z = 0$), which in turn depends on $n_{a\pm}$ through the boundary condition imposed on $\varphi_0(z)$, *i.e.*, $\partial_z\varphi_0(z)|_{z=0} = -(\ell_B/2)[n_0/Z - (pn_{a+} - n_{a-})]$. Thus, $n_{a\pm}$ can be determined from eq. (13) self-consistently as a function of the bare surface charge and κ, which is related to the salt concentration in the bulk. Note that eq. (13) depends only on a single important parameter, which will be called the charge regulation parameter,

$$\tau \equiv \frac{Z(pn_{a+} - n_{a-})}{n_0}. \quad (17)$$

It expresses the fraction of how much of the bare surface charge has been modified due to charge regulation. Thus, combining n_{a+} and n_{a-} from eq. (13), we obtain

$$\tau_{\mathrm{MF}} = \frac{gs^2}{4(1+p)}\left[b_+e^{p\varphi_0(0)} - b_-e^{-\varphi_0(0)}\right], \quad (18)$$

where we have defined dimensionless parameters $b_\pm \equiv e^{\varepsilon_\pm}a_\pm^3/(\ell_B\,a_{c\pm}^2)$, $g \equiv \ell_B/\lambda$ is the coupling constant, $s \equiv \kappa\lambda$, and $\lambda \equiv 4Z/(n_0\ell_B)$ is the Gouy-Chapman length. We will examine the charge regulation parameter and other physical quantities such as the adsorption isotherms in the mean-field approximation in sect. 3.

2.3 The Green's function, one-loop corrections to the electrostatic potential, and the one-loop ion distributions

To go beyond the mean-field description for $n_{a\pm}$, we have to compute the one-loop corrections to the chemical potentials for the ions, which are related to $\delta\Lambda_\pm$ and $\delta\Lambda_{a\pm}$, as

appeared in eq. (15). First, we have to obtain expressions for the one-loop corrections to the electrostatic potential $\langle[\imath\Delta\psi(\mathbf{x})]\rangle_1$ and the one-loop ion distributions $\langle\hat{\rho}_{\pm}(\mathbf{x})\rangle_1$ and $\langle\hat{\rho}_{a\pm}(\mathbf{x})\rangle_1$. Following ref. [8], it is straightforward to obtain a formal expression for $\langle[\imath\Delta\psi(\mathbf{x})]\rangle_1$:

$$\langle[\imath\Delta\psi(\mathbf{x})]\rangle_1 = \frac{1}{\ell_B}\int \mathrm{d}^3\mathbf{x}'\, G(\mathbf{x},\mathbf{x}') \times\left[\frac{1}{2}\,H(\mathbf{x}')\,G(\mathbf{x}',\mathbf{x}') - F(\mathbf{x}')\right], \tag{19}$$

where $F(\mathbf{x}')$ and $H(\mathbf{x}')$ are given by eqs. (15) and (16), respectively, $G(\mathbf{x},\mathbf{x}')$ is the Green's function, which is the inverse of the operator $K(\mathbf{x},\mathbf{x}')$ of eq. (14), and it satisfies

$$\left\{-\nabla^2_{\mathbf{x}} + \frac{\kappa^2}{1+p}\left[p\,e^{p\varphi_0(\mathbf{x})} + e^{-\varphi_0(\mathbf{x})}\right] + \frac{2}{\lambda_D}\,\delta(z)\right\} G(\mathbf{x},\mathbf{x}') = \ell_B\delta(\mathbf{x}-\mathbf{x}'). \tag{20}$$

Physically, the Green's function can be interpreted as the electrostatic interaction between two unit charges located at $\mathbf{x}$ and $\mathbf{x}'$ in the presence of the charged surface with its accompanying free and adsorbed ions. (For a more complete discussion of the Green's function, see appendix A.1.) Using the property of the Green's function, eq. (19) can be cast into the differential equation

$$\left\{-\nabla^2_{\mathbf{x}} + \frac{\kappa^2}{1+p}\left[p\,e^{p\varphi_0(\mathbf{x})} + e^{-\varphi_0(\mathbf{x})}\right] + \frac{2}{\lambda_D}\,\delta(z)\right\}\langle[\imath\Delta\psi(\mathbf{x})]\rangle_1 = \frac{1}{2}\,G(\mathbf{x},\mathbf{x})H(\mathbf{x}) - F(\mathbf{x}). \tag{21}$$

By the same token, the one-loop ion distributions for the positive and negative free ions and the positive and negative adsorbed ions, respectively, can be obtained to give

$$\langle\hat{\rho}_{\pm}(\mathbf{x})\rangle_1 = \frac{\kappa^2 e^{\pm(Z_\pm/Z)\varphi_0(\mathbf{x})}}{(Z_\pm/Z)(1+p)\ell_B}\left\{1 \pm (Z_\pm/Z)\langle[\imath\Delta\psi(\mathbf{x})]\rangle_1 - \frac{1}{2}(Z_\pm/Z)^2\,G(\mathbf{x},\mathbf{x}) + \frac{\delta\Lambda_\pm}{\Lambda^{(0)}_\pm}\right\}, \tag{22}$$

$$\langle\hat{\rho}_{a\pm}(\mathbf{x})\rangle_1 = n_{a\pm}\delta(z)\left\{1 \pm (Z_\pm/Z)\langle[\imath\Delta\psi(\mathbf{x})]\rangle_1 - \frac{1}{2}(Z_\pm/Z)^2\,G(\mathbf{x},\mathbf{x}) + \frac{\delta\Lambda_{a\pm}}{\Lambda^{(0)}_{a\pm}}\right\}. \tag{23}$$

The parameters $\delta\Lambda_\pm$ and $\delta\Lambda_{a\pm}$ and hence, the one-loop corrections to the chemical potentials can be determined by three conditions. i) We require that at the one-loop level, $\langle\hat{\rho}_{a\pm}(\mathbf{x})\rangle_1 = n_{a\pm}\delta(z)$. This condition merely expresses the definition of $n_{a\pm}$. ii) We impose the following boundary conditions on $\langle[\imath\Delta\psi(\mathbf{x})]\rangle_1$: (a) $\langle[\imath\Delta\psi(z)]\rangle_1 \to 0$ as $|z|\to\infty$, and (b) $\partial_z\langle[\imath\Delta\psi(z)]\rangle_1|_{z=0} = 0$, as dictated by charge neutrality at one loop. iii) We demand that all the infinite self-energy terms must be canceled at the one-loop level, leaving $\langle[\imath\Delta\psi(\mathbf{x})]\rangle_1$ and $\langle\hat{\rho}_{\pm}(\mathbf{x})\rangle_1$ perfectly finite.

First, we see from eq. (23) that condition i) implies that

$$\frac{\delta\Lambda_{a\pm}}{\Lambda^{(0)}_{a\pm}} = \mp\,(Z_\pm/Z)\,\langle[\imath\Delta\psi(0)]\rangle_1 + \frac{1}{2}\,(Z_\pm/Z)^2\,G(0,0). \tag{24}$$

Next, let us consider conditions ii) and iii). It is convenient to split the self-energy, $G(\mathbf{x},\mathbf{x})$, which is just the diagonal part of the Green's function, appearing in eqs. (21)–(23), into three contributions (see appendix A.1):

$$G(\mathbf{x},\mathbf{x}) = 2V_0 - \frac{\ell_B\kappa}{4\pi} + \mathcal{G}(z,z), \tag{25}$$

where $V_0 \equiv \frac{\ell_B}{2}\int\frac{\mathrm{d}^2\mathbf{q}}{(2\pi)^2}\frac{1}{2q}$ is the bare (infinite) self-energy, the second term is the Debye-Huckel contribution, which comes from the charge fluctuations in the bulk [8], and the last term, $\mathcal{G}(z,z)$, represents the self-energy of an ion in the presence of the charged surface (along with the ions associated with it) at distance z away from it. Note that $\mathcal{G}(z,z)$ has the property that $\mathcal{G}(z,z)\to 0$ when $z\to\infty$ (see appendix A.1). Thus, we see that eqs. (21) and (22) contain the infinite self-energy terms and that $\langle[\imath\Delta\psi(z)]\rangle_1$ does not go to zero as $z\to\infty$, as can be seen from eq. (21). By inspecting eqs. (21) and (22), it is clear we must choose $\delta\Lambda_\pm$ to be

$$\frac{\delta\Lambda_\pm}{\Lambda^{(0)}_\pm} = V_0^{\pm} - (Z_\pm/Z)^2\left(\frac{\ell_B\kappa}{8\pi}\right). \tag{26}$$

Indeed, substituting eqs. (24) and (26) in $F(\mathbf{x})$, eq. (21) becomes

$$\left\{-\partial_z^2 + \frac{\kappa^2}{1+p}\left[p\,e^{p\varphi_0(z)} + e^{-\varphi_0(z)}\right]\right\}\langle[\imath\Delta\psi(z)]\rangle_1 = \frac{\kappa^2}{2(1+p)}\,\mathcal{G}(z,z)\left[p^2 e^{p\varphi_0(z)} - e^{-\varphi_0(z)}\right], \tag{27}$$

which has the desirable behavior that $\langle[\imath\Delta\psi(z)]\rangle_1 \to 0$ at $|z|\to\infty$. In order to solve for $\langle[\imath\Delta\psi(z)]\rangle_1$, we need another boundary condition. This can be obtained from the charge neutrality condition (see eq. (7)) at one loop:

$$\int \mathrm{d}^3\mathbf{x}\left\{\left[p\,e^{p\varphi_0(\mathbf{x})} + e^{-\varphi_0(\mathbf{x})}\right]\langle[\imath\Delta\psi(\mathbf{x})]\rangle_1 - \frac{1}{2}\,\mathcal{G}(\mathbf{x},\mathbf{x})\left[p^2 e^{p\varphi_0(\mathbf{x})} - e^{-\varphi_0(\mathbf{x})}\right]\right\} = 0, \tag{28}$$

where we have made use of eqs. (22), (23), (24), and (26). Equation (28) implies, with the help of eq. (27), that

$$\int_{-\infty}^{\infty}\mathrm{d}z\,\partial_z^2\langle[\imath\Delta\psi(z)]\rangle_1 = 0, \tag{29}$$

which in turn implies that $\partial_z\langle[\imath\Delta\psi(z)]\rangle_1|_{z=0} = 0$. This boundary condition simply states that fluctuations do not modify the bare surface charge density. (For a more complete discussion of $\langle[\imath\Delta\psi(z)]\rangle_1$, see appendix A.2.)

2.4 Adsorbed ion surface densities at one loop

Now, equating the (one-loop) chemical potentials for the free ions

$$\mu_{\pm}^{(1)} = -V_0^{\pm} + \ln\left[\frac{\Lambda_{\pm}^{(0)} a_{\pm}^3}{\ell_B}\right] + \frac{\delta\Lambda_{\pm}}{\Lambda_{\pm}^{(0)}}\,, \tag{30}$$

to the (one-loop) chemical potentials for the adsorbed ions

$$\mu_{a\pm}^{(1)} = -\varepsilon_{\pm} - V_0^{\pm} + \ln\left[\frac{\Lambda_{a\pm}^{(0)}\, a_{c\pm}^2}{\ell_B}\right] + \frac{\delta\Lambda_{a\pm}}{\Lambda_{a\pm}^{(0)}}\,, \tag{31}$$

and making use of eqs. (13), (24), and (26) (note that all the bare self-energies, $V_0^{\pm}$, cancel out nicely), we find the equilibrium values for n_{a+} and n_{a-} at the one-loop level to be

$$\begin{aligned} n_{a+} &= \frac{\kappa^2\, b_+}{p(1+p)} e^{p\varphi_1(0) - p^2\mathcal{G}(0,0)/2}, \\ n_{a-} &= \frac{\kappa^2\, b_-}{1+p} e^{-\varphi_1(0) - \mathcal{G}(0,0)/2}. \end{aligned} \tag{32}$$

where $\varphi_1(0) \equiv \varphi_0(0) + \langle[\imath\Delta\psi(0)]\rangle_1$ is the one-loop electrostatic potential at the plate.

Equation (32) is the central result of this paper, and we will present a thorough discussion of its predictions for the adsorption isotherms in sect. 4. Here, we should make a few remarks. First, eq. (32) have the same functional form as that of the mean-field approximation given by eq. (13), except with the electrostatic potential and self-energies (both evaluated at the plate $z = 0$) replaced by their one-loop counterparts[3]. In particular, since $\mathcal{G}(0,0) < 0$, the self-energies may be viewed as giving rise to an effective binding energy.

Secondly, in the limit $\ell_B \to 0$, *i.e.*, when electrostatic interaction is turned off, eq. (32) reduces to

$$n_{a+} = \frac{\wp\, a_+^3}{a_{c+}^2}\frac{e^{\varepsilon_+}}{1+p}\,, \qquad \text{and} \qquad n_{a-} = \frac{\wp\, a_-^3}{a_{c-}^2}\frac{p\, e^{\varepsilon_-}}{1+p}\,,$$

where $\wp = \kappa^2/(p\,\ell_B)$ is the ideal gas pressure (in units of k_BT) in the bulk (see appendix A.3). In particular, if we set $\varepsilon_+ = \varepsilon_-$ and $a_+^3/a_{c+}^2 = a_-^3/a_{c-}^2$, then $n_{a+} + n_{a-} = \wp\, a_+^3 e^{\varepsilon_+}/a_{c+}^2$, reproducing, as it should, the adsorption isotherms of Henry's law, which describes the absorption of gas molecules onto a substrate when there is no interaction among the absorbed molecules [41]. Note that in this limit the number of absorbed particles scales linearly with pressure in the bulk.

Third, according to eq. (32), the Green's function in eq. (20) and the one-loop corrections to the electrostatic potential in eq. (27) must be solved explicitly in order to obtain $n_{a\pm}$. This means that $n_{a\pm}$ now depend also on the combination, $2/\lambda_D = \ell_B(p^2 n_{a+} + n_{a-})$, through its dependence on the Green's function in eq. (20). Thus, unlike the mean-field theory, eqs. (32) cannot be combined, so that it depends only on a single parameter. Furthermore, $G(\mathbf{x},\mathbf{x}')$ and $\langle[\imath\Delta\psi(\mathbf{x})]\rangle_1$ can only be solved for the cases where the exact solution to the PB equation, eq. (10), is known. To the best of our knowledge, eq. (10) can only be solved for the cases where $p = 1$ and $p = 2$, and we will consider these two important cases in sect. 4[4]. Because of the mathematical complexity, we relegate most of the mathematical details to appendix A, which includes an explicit construction of the Green's function and the solution to one-loop corrections to the electrostatic potential $\langle[\imath\Delta\psi(\mathbf{x})]\rangle_1$, and a calculation of the one-loop free energy. It should be noted that eq. (32) can also be obtained by minimizing the 1-loop surface free energy, eq. (A.43), with respect to $n_{a\pm}$, as it should be.

Finally, we end this section by pointing out an important technical detail, which concerns the fact that $\mathcal{G}(0,0)$ in eqs. (32) diverges logarithmically in the ultraviolet limit. This divergence arises from charge fluctuations of a Coulomb gas confined to a plane, which is well known [45]. Indeed, we can decompose $\mathcal{G}(z,z)$ as a sum of two contributions $\mathcal{G}(z,z) = \mathcal{G}_{2d}(z,z) + \mathcal{G}_{3d}(z,z)$, where $\mathcal{G}_{3d}(z,z)$ represents the self energy of the free ions (see appendix A.1) and $\mathcal{G}_{2d}(z,z)$ arises from the fluctuations of the adsorbed ions, given by

$$\mathcal{G}_{2d}(z,z) = -\frac{\ell_B}{4\pi}\int_{\kappa}^{\infty} \mathrm{d}q\, \frac{e^{-2q|z|}}{1+q\lambda_D}\,. \tag{33}$$

This is the self-energy of a Coulomb gas confined to a plane immersed in an electrolyte solution. While $\mathcal{G}_{3d}(0,0)$ is perfectly finite, $\mathcal{G}_{2d}(0,0) \sim \int \mathrm{d}q/q$, diverges logarithmically in the upper limit. To regulate this divergence, we choose an upper cut-off $\sim 2\pi/a$, inversely proportional to the size of an ion[5].

3 Charge regulation at mean field

In this section, we explore charge regulation of a charged planar surface at the mean-field level as given by eqs. (13) and (18). Since we expect that the mean-field theory should be valid when the surface charge density is not too high and additionally, it may serve as a guide when we compare our results with those from sect. 4, where we discuss correlation effects, a discussion of the mean-field theory is, therefore, not without interest. We first present the two cases ($p = 1$ and 2) where exact solutions to PB equation are known, then we move on to consider the general case of arbitrary p.

The exact solutions for the PB equation, eq. (10), for $p = 1$, *i.e.*, (Z,Z)-electrolyte [1], and $p = 2$, *i.e.*,

[3] Technically, the self-energy at mean field is given by the (infinite) bare self-energy $V_0^{\pm}$. However, they are cancelled out, even at the mean-field level and do not appear in eq. (13). In this sense, we can take the self-energy at mean field to be zero.

[4] Note that there is a symmetry between the case $p = 1/2$ and $p = 2$. We will not consider such a case in this paper.

[5] The upper cut-off is, of course, somewhat arbitrary and the present continuum treatment cannot make a rigorous identification of this quantity.

$(2Z, Z)$-electrolyte [46], can be written as

$$\varphi_0(z) = \begin{cases} 2\ln\left[\dfrac{1+\gamma_1\, e^{-\kappa|z|}}{1-\gamma_1\, e^{-\kappa|z|}}\right], & \text{for } p=1, \\ \ln\left[\dfrac{\left(1+\gamma_2\, e^{-\kappa|z|}\right)^2}{1-4\gamma_2\, e^{-\kappa|z|}+\gamma_2^2\, e^{-2\kappa|z|}}\right], & \text{for } p=2. \end{cases} \tag{34}$$

The constants, γ_1 and γ_2, are determined by the boundary condition imposed on the electric field at the plate: $\partial_z\varphi_0(z)|_{z=0} = -2(1-\tau)/\lambda$, where τ, defined in eq. (18), is the charge regulation parameter that measures the extent to which the charged plate has been modified due to charge regulation, and $\lambda \equiv 4Z/(n_0\ell_B)$ is the Gouy-Chapman length. Defining $s \equiv \kappa\lambda$, we can write γ_1 as

$$\gamma_1 = \frac{\sqrt{(1-\tau)^2+s^2}-s}{1-\tau}, \tag{35}$$

and we can determine γ_2 from the equation

$$\frac{3s}{1-\tau} = 2 + \frac{4}{1-\gamma_2} + \frac{1}{\gamma_2} - \gamma_2, \tag{36}$$

which can be solved exactly (see appendix B). When $\tau > 1$, *i.e.*, when the plate becomes oppositely (positive) charged, γ_p becomes negative and eq. (34) remains valid with negative γ_p. Note that for $p = 1$, $\varphi_0(z) \to -\varphi_0(z)$, when $\gamma_1 \to -\gamma_1$, but for $p = 2$, $\varphi_0(z)$ does not enjoy this symmetry, because of the underlying asymmetry in the valences of the ions. Using eqs. (34), the mean-field electrostatic potential at $z = 0$ can readily be found in terms of γ_p. Substituting the results into eq. (18) and considering the simple case of $b_+ = b_- = b$, we find a non-linear relation for the charge regulation parameter:

$$\tau = \begin{cases} \dfrac{gb}{2}(1-\tau)\sqrt{s^2+(1-\tau)^2}, & \text{for } p=1, \\ \dfrac{gb}{6}\,\gamma_2(1-\tau)^2\left[1+\dfrac{1}{\gamma_2^2}+\dfrac{4}{(1-\gamma_2)^2}\right], & \text{for } p=2, \end{cases} \tag{37}$$

where $g \equiv \ell_B/\lambda$ and $s \equiv \kappa\lambda$. Note that g is proportional to the bare surface charge density n_0.

In fig. 2, we plot τ as a function of g, for a fixed $\kappa\ell_B$, *i.e.* constant salt concentration. We observe that τ increases with g for small g but saturates to $\tau \sim 1$ when g is large. This behavior is expected since as the charge density of the plate increases, it creates a stronger electric force which binds the positive ions to the plate, effectively neutralizing the plate. This happens slowly until the plate is completely neutralized. Indeed, as $g \to \infty$, we find that τ approaches 1 as slowly as $1-\tau \sim 1/\sqrt{g}$ for both $p = 1$ and 2. This slow decay may be attributed to the general characteristics of charged systems. Note also that the mean-field theory predicts that there is no charge inversion for the case $b_+ = b_-$, even for divalent ions ($p = 2$). As can be seen from fig. 2, divalent ions are indeed more efficient at neutralizing the charged surface, but τ exhibits qualitatively similar behavior for both monovalent ($p = 1$) and divalent ($p = 2$) ions. In the opposite limit, $g \ll 1$, we find $\tau = \kappa\ell_B b/(2+\kappa\ell_B b) + \mathcal{O}(g)$ approaches a finite value. This means, in particular, that the charged surface is always renormalized, due to charge regulation, by a finite amount: $n_0(1-\tau) \approx n_0/(1+\kappa\ell_B b/2)$. Note that this result is independent of p (see below).

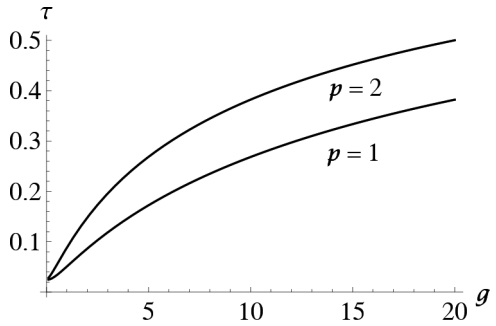

Fig. 2. The charge regulation parameter τ as a function of $g = \ell_B/\lambda$ for $\kappa\ell_B = 0.5$ and $b_+ = b_- = b = 0.1$ as determined by the mean-field equation, eq. (37). τ starts out at a finite value and increases slowly as g (bare surface charges) increases, but never crosses beyond 1. Note that divalent counterions are more efficient in neutralizing the plate, but exhibit qualitatively similar behavior to that of monovalent courterions.

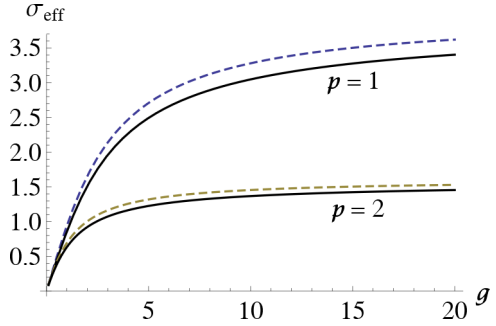

Fig. 3. The effective charge σ_{eff} as a function of g for $\kappa\ell_B = 2$ and $b_+ = b_- = b = 0.1$ for $p = 1$ and $p = 2$. The dashed lines represent the case where charge regulation is turned off, *i.e.* $\tau = 0$. It is clear that charge regulation lowers the effective charge. Note that the asymptotic values of σ_{eff} at large g for $p = 1$ and $p = 2$ are $\sigma_{\text{eff}} = 4$ and $\sigma_{\text{eff}} = 6(2-\sqrt{3})$, respectively.

In order to discern the importance of charge regulation at the mean-field level, we examine another interesting quantity, namely, the effective charge σ_{eff} [47]. It is defined through the asymptotic behavior of the electrostatic potential as $|z| \to \infty$: $\varphi_0(z) \sim \sigma_{\text{eff}}\, e^{-\kappa|z|}$. From eq. (34), it is easy to see that

$$\sigma_{\text{eff}} = \frac{4s}{1-\tau}\left[\sqrt{1+\frac{(1-\tau)^2}{s^2}}-1\right] \tag{38}$$

for $p = 1$, and $\sigma_{\text{eff}} = 6\gamma_2$ for $p = 2$. In the absence of charge regulation, *i.e.*, setting $\tau = 0$, $\sigma_{\text{eff}} \sim 2/s$ is proportional to the bare surface charge n_0 when it is low, $s \gg 1$, for both $p = 1$ and $p = 2$. When the bare surface charge is high $s \ll 1$, $\sigma_{\text{eff}} \simeq 4$ ($p = 1$) and $\sigma_{\text{eff}} \simeq 6(2-\sqrt{3}) \approx 1.607$ ($p = 2$), and thus, the effective charge approaches to a

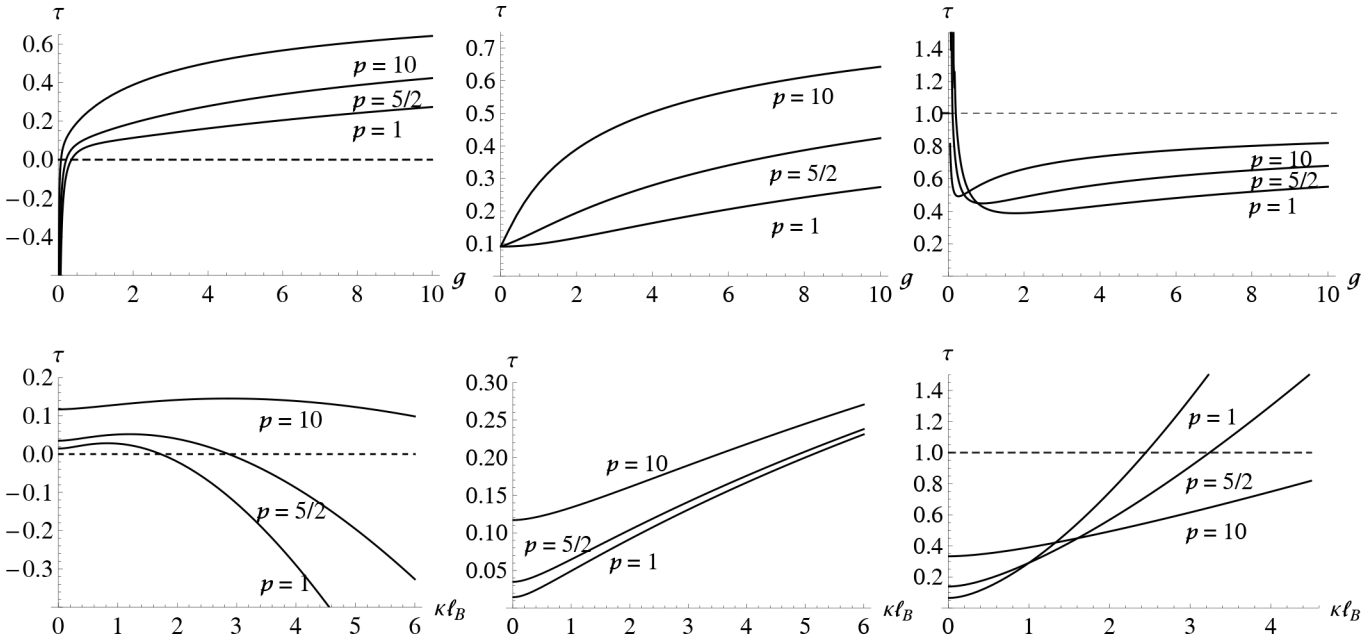

Fig. 4. The charge regulation parameter τ as a function of g (at a constant $\kappa\ell_B = 2$) (top) and $\kappa\ell_B$ (at a constant $g = 0.3$) (bottom) with different $p = 1, 5/2$, and 10, for three different cases: i) $b_- > b_+$ (left) with $b_+ = 0.1$ and $b_- = 0.2$, ii) $b_+ = b_- = 0.1$ (center), and iii) $b_+ > b_-$ (right) with $b_+ = 0.5$ and $b_- = 0.1$. It is interesting to observe that at constant surface charge, τ increases initially at small salt concentration but decreases at higher salt concentration in case i) (left, bottom), and charge inversion can be achieved at a high salt concentration even at the mean-field level in case iii) (right, bottom).

constant value independent of the bare surface charge as a result of charge renormalization [47]. In fig. 3, we plot the effective charge σ_{eff} as a function of g for both $p = 1$ and $p = 2$. We observe that charge regulation, as expected, lower the effective charge somewhat, with the difference more pronounced for higher salt concentration. However, the effective charge still goes to their asymptotic values, albeit more slowly, indicating that the charge regulation does not have a drastic effect at the mean-field level.

Next, we consider the general case of arbitrary p. Although the exact solution to the PB equation is not known for general p, it turns out that $n_{a\pm}$ can still be determined in the mean-field theory because $\varphi_0(0)$ can be obtained without solving $\varphi_0(z)$ explicitly. To see this, we multiply eq. (10) by $\partial_z\varphi_0(z)$, integrate over z, and note that the left-hand-side of the equation

$$-\frac{1}{2}\left[\partial_z\varphi_0(z)\right]^2 + \frac{\kappa^2}{p(1+p)}\left[e^{p\varphi_0(z)} + p\,e^{-\varphi_0(z)}\right] = \frac{\kappa^2}{p}\,,$$

is a constant for all z. Thus, using the boundary condition for $\partial_z\varphi_0(z)$ at the plate, we find

$$1 + \frac{2\,p(1-\tau)^2}{s^2} = \frac{e^{p\varphi_0(0)} + p\,e^{-\varphi_0(0)}}{1+p}\,. \tag{39}$$

Together with eq. (18),

$$\tau_{\text{MF}} = \frac{gs^2}{4(1+p)}\left[b_+ e^{p\varphi_0(0)} - b_- e^{-\varphi_0(0)}\right],$$

the charge regulation parameter τ can be determined uniquely. Though it may be difficult to solve $e^{\varphi_0(0)}$ from eq. (39) in a closed form since it involves finding the roots of a polynomial of order $p+1$, it is straightforward to solve these coupled non-linear equations numerically.

Recall that τ represents how much the bare surface charges have been modified. When $\tau < 0$, there are more negative than positive charges are adsorbed, making the surface more negatively charged. On the other hand, when $\tau > 0$, there are more positive ions than negative ions adsorbed onto the charged plate, partially neutralizing it. In particular, $\tau > 1$ represents overcharging or charge inversion, where the plate switches from negatively to positively charged.

In fig. 4, we plot τ as a function of g (at a fixed $\kappa\ell_B$) and $\kappa\ell_B$ (at a fixed g) for $p = 1$, 5/2, and 10 in the regions mentioned above: i) $b_- > b_+$, ii) $b_- = b_+$, and iii) $b_+ > b_-$. In case i), where the binding energy of the negative ions is greater than that of the positive ions, the negative ions are being adsorbed onto an almost neutral surface at a constant salt concentration. Thus, $\tau < 0$ for $g \ll 1$. As the surface becomes more negatively charged, a stronger electric field binds the positive ions and effectively neutralizing the surface and $\tau > 0$. This occurs when $g > [\kappa\ell_B/(2+2p)]\ln(b_-/b_+)$. On the other hand, when the salt concentration is increased at a constant surface charge, τ increases slightly with $\kappa\ell_B$ for small $\kappa\ell_B$, but as $\kappa\ell_B$ increases, more negative ions are available to bind to the surface, and τ reverses course and decreases as salt concentration increases, and eventually, $\tau < 0$ when $\kappa\ell_B > 2g(1+p)/\ln(b_-/b_+)$.

In case ii) where $b_+ = b_- = b$, τ behaves qualitatively the same as the $p = 1$ and 2 cases studied above with

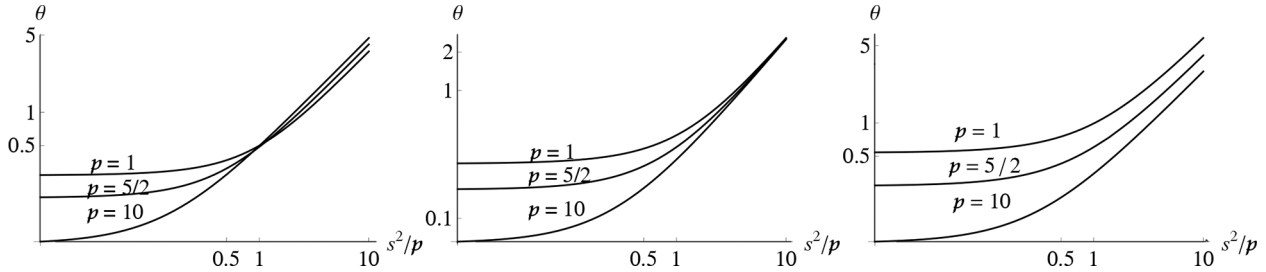

Fig. 5. A log-log plot of the coverage $[\theta \equiv Z(n_{a+} + n_{a-})/n_0]$ *vs.* dimensionless pressure $[\wp\, \ell_B \lambda^2 = s^2/p]$ with different $p = 1$, 5/2, and 10, at a fixed $g = 10$, for three different cases: i) $b_- > b_+$ (left) with $b_+ = 0.1$ and $b_- = 0.2$, ii) $b_+ = b_- = 0.1$ (center), and iii) $b_+ > b_-$ (right) with $b_+ = 0.5$ and $b_- = 0.1$. These curves represent adsorption isotherms of ions on a charged plate as predicted by the mean-field theory, given by eq. (40). Note that in all cases θ varies linearly with $\wp$ at large $\wp$.

the exact solutions to the PB equation. At a constant salt concentration, $\tau = \kappa\ell_B b/(2+\kappa\ell_B b)+(p-1)gb/(2+\kappa\ell_B)^3$, for $g \ll 1$, and $\tau \sim 1 - \sqrt{2/(gbp)}$ for $g \gg 1$. Note that for $g \ll 1$, the charge regulation parameter at $g = 0$ is independent of p, but the slope scales with p, as can be seen in fig. 4 (center, top). At a constant surface charge, $\tau \approx 1 + (1 - \sqrt{1 + 2gbp})/(gbp)$ for $\kappa\ell_B \ll 1$, and $\tau \sim 1 - 2/(\kappa\ell_B b)$ for $\kappa\ell_B \gg 1$. In case iii), where the binding energy of the positive ions is greater than that of the negative ions, the positive ions are being adsorbed onto an almost neutral surface at a constant salt concentration. Thus, $\tau > 1$ for $g \ll 1$, and τ decreases rapidly, as the surface becomes negatively charged $\tau < 1$. Then, τ increases as positive ions start to neutralize the plate and eventually τ reaches an asymptotic values for large g. At a constant surface charge, τ increases monotonically with salt concentration, and crosses the charge inversion threshold of $\tau > 1$. This occurs when $\kappa\ell_B > 2\sqrt{g(1+p)/(b_+ - b_-)}$, as more positive ions preferably bind to the surface, changing the surface from a negatively charged surface to a positively charged surface.

Finally, we calculate the adsorption isotherm for this system at the mean-field level. The adsorption isotherm is defined by the coverage, $\theta \equiv Z(n_{a+} + n_{a-})/n_0$, as a function of the pressure in the bulk, $\wp = \kappa^2/(p\ell_B)$. Physically, the coverage θ measures how much materials are adsorbed on the charged plane. Using eq. (13), it is straightforward to show that the coverage is given by

$$\theta = \frac{gs^2}{4p(1+p)} \left[b_+ e^{p\varphi_0(0)} + p\, b_- e^{-\varphi_0(0)} \right]. \qquad (40)$$

Note at the mean-field level that θ is not an independent variable. Rather, it is slaved to the charge regulation parameter τ, through its dependence on $\varphi_0(0)$. Indeed, for the simple case of $b_+ = b_- = b$, θ can be expressed solely in terms of τ:

$$\theta = \frac{gb}{4} \left[\frac{s^2}{p} + 2\,(1-\tau)^2 \right].$$

In fig. 5, we plot $Z\theta$ as a function of the dimensionless pressure $\wp\, \ell_B \lambda^2 = s^2/p$ for case i), ii), and iii). We observe that at low pressure, θ is almost flat, but at high pressure, θ scales linearly with $\wp$, as can be easily seen from the above equation. The latter behavior is nothing but Henry's law [41], which implies the absence of interactions among the adsorbed ions at the mean-field level. This will be rectified in the next section by considering correlation effects.

4 Charge regulation at one loop

In this section, we present the central results of this paper, namely, charge regulation of a planar surface at the one-loop level, as given by eq. (32). As we saw in sect. 3, the mean-field predictions for the absorption isotherms are rather straightforward, even for large p, with the charge regulation parameter τ and the coverage θ vary smoothly with system parameters such as the bare surface charge and salt concentrations. However, when correlation effects are taken into account at the one-loop level, the physics of charge regulation is drastically altered. This is not entirely surprising because correlation effects include many-body interactions among the ions (adsorbed or otherwise), and we might expect phase transitions to occur [48].

Indeed, let us consider an analogous problem: the absorption of gas molecules onto a two-dimensional substrate with sticky sites. If we assume for the moment that there is no interaction among the absorbed molecules other than particle exclusion, *i.e.*, no two molecules can occupy the same site, then at equilibrium, the number of molecules adsorbed is described by the Langmuir isotherm, with the coverage varies linearly with the pressure of the gas, when the pressure is low, and approaches unity, when the pressure is high [32]. However, the assumption that there is no interaction among absorbed molecules may not always be applicable, especially when the coverage gets moderately high. In fact, experimental measurements show that under the right conditions the absorption isotherms exhibit discontinuities, indicating a first-order phase transition [49]. This first-order phase transition has been rationalized by Fowler, who used a two-dimensional lattice-gas model with the nearest neighbors attraction to describe the interaction among the absorbed molecules, and within the Williams-Bragg (mean-field) approximation, he showed that the adsorption isotherm exhibits a liquid-gas–like transition with a critical point [50].

Similar consideration can be applied to the present problem of charge regulation, which can be viewed, in part, as the adsorption of ions onto a charged surface. When the surface charge is low, the number of ions (both positive and negative) absorbed is low, and, therefore, correlation effects are negligible. In this case, the ions can be treated as an ideal gas and the behavior of the adsorption isotherms may well be described by the mean-field theory, in which the coverage varies linearly with the pressure, reflecting precisely the non-interacting nature of this regime (see fig. 5). However, when the number of ions absorbed increases, correlation effects that lead to an effective interaction among the absorbed ions, can no longer be neglected. To a good approximation, this effective interaction may be described by the well-known Green's function for a Coulomb gas confined to a plane,

$$G_{2d}(\mathbf{r},0) = \int \frac{\mathrm{d}^2\mathbf{q}}{(2\pi)^2}\,\frac{\ell_B}{2\alpha\kappa}\left[1-\frac{1}{1+\alpha\kappa\lambda_D}\right] e^{\imath\mathbf{q}\cdot\mathbf{r}}, \quad (41)$$

which is different from the 3D counterpart as given by the Debye-Huckel screened potential (Yukawa potential) [51], and eq. (41) constitutes a dipolar-like ($\sim 1/r^2$) interaction among the adsorbed ions of both signs, giving rise to a phase transition similar to the 2d lattice gas model mentioned above. Indeed, this has been suggested before for the counterion-only case [48]. Note also that charge regulation may lead to phase transitions in other charged systems as well [33–35].

Here, we present the adsorption phase diagrams for $p = 1$, symmetric electrolyte, and $p = 2$, asymmetric electrolyte. For simplicity, we keep the number of system parameters to a minimum by focusing on the important case where $\varepsilon_\pm = 0$ and $a_\pm^3/a_{c\pm}^2 = a$. Physically, this scenario describes the self-regulation of a charged surface by the electrostatic interaction alone. As we will see below, this simplest case is already highly non-trivial. In particular, we find that the phase diagrams for $p = 1$ and $p = 2$ are quite distinct, suggesting that the physics of charge regulation is no longer universal but crucially depends on the valency of the ions.

To construct the phase diagrams, it may be more convenient to use the charge regulation parameter $\tau \equiv Z(pn_{a+}-n_{a-})/n_0$ and the coverage $\theta \equiv Z(n_{a+}+n_{a-})/n_0$. Using eq. (32), it is straightforward to obtain the coupled non-linear equations for τ and θ as

$$\tau = \frac{gbs^2}{4(1+p)}\left(e^{p\varphi_s - p^2\mathcal{G}_s/2} - e^{-\varphi_s-\mathcal{G}_s/2}\right), \quad (42)$$

$$\theta = \frac{gbs^2}{4p(1+p)}\left(e^{p\varphi_s - p^2\mathcal{G}_s/2} + p\,e^{-\varphi_s-\mathcal{G}_s/2}\right), \quad (43)$$

where $s \equiv \kappa\lambda$, $\varphi_s \equiv \varphi_0(0) + \langle[\imath\Delta\psi(0)]\rangle_1$, the mean-field potential $\varphi_0(z)$ is given by eq. (34), the one-loop corrections to the electrostatic potential, $\langle[\imath\Delta\psi(0)]\rangle_1$, is given by eq. (A.25), and $\mathcal{G}_s \equiv \mathcal{G}(0,0)$, given in eq. (A.11), may be interpreted as the effective binding energy. Note that φ_s and $\mathcal{G}_s$ are functions of τ and θ, as well as a set of system parameters: the coupling constant, $g \equiv \ell_B/\lambda$, which is proportional to the bare surface charge, $\kappa\ell_B$, which is proportional to the salt concentration, and $b \equiv a/\ell_B$, which is proportional to the temperature of the system. The phase diagram is constructed according to the nature of the solution to eqs. (42) and (43). If only one solution (τ,θ) is found at a given g, $\kappa\ell_B$, and b, it represents a homogeneous phase. If n solutions (τ_1,θ_1), (τ_2,θ_2), ..., are found with the same surface free energy (see appendix A.3, eq. (A.43)), they represent n homogeneous phases at equilibrium.

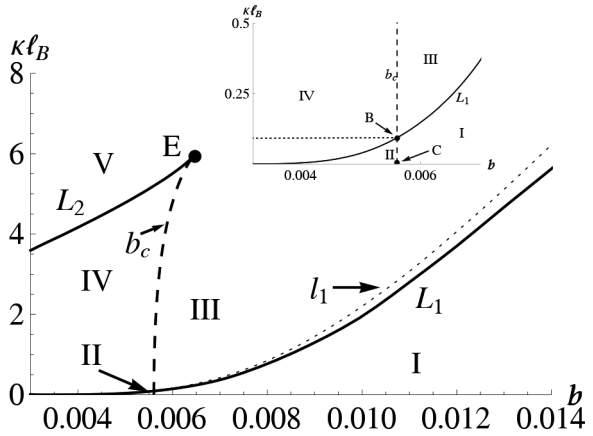

Fig. 6. Phase diagram for symmetric $(1,1)$ electrolyte in the $(\kappa\ell_B, b)$-plane. It is divided into 5 regions. Region I is the single-phase region, Region II, III, and V are the two-phase regions, and Region IV is the three-phase region. A line of critical points, labeled as b_c, beginning at point C $\equiv (0.0056, 0)$ (see inset) and ending at point E $\equiv (0.0064, 5.9)$, separates Region I and II below the L_1 line, and Regions III and IV above the L_1 line. The L_1 line is a first-order line which interacts the b_c line at $B \equiv (0.0057, 0.1)$, and delineates the low salt from the high salt behavior of the system. At low temperature, $b < b_c$, the L_1 line separates the low salt region (Region II), from the intermediate salt region (Region IV). Another first-order line, the L_2 line, separates Region IV from the high salt region (Region V). The L_2 line and b_c line end together at E, a critical endpoint. The dotted line, labeled as l_1, does not represent a phase boundary. Rather, it delineates the existence of a solution (to eqs. (42) and (43)) characterized by $\tau \approx 1$ in the limit when the surface charge vanishes.

4.1 Phase diagram for symmetric (1, 1) electrolyte

In this section, we present the phase diagram for symmetric $(1,1)$ electrolyte. Since we have three system parameters, g, $\kappa\ell_B$, and b, the phase diagram should be three dimensional. However, to capture the system behavior as the surface charge varies, it is sufficient to project the phase diagram onto the $(\kappa\ell_B, b)$-plane, which is depicted in fig. 6. This phase diagram is divided into 5 regions. Region I is the high-temperature ($b > b_c$), low salt (below L_1 line) regime, where the adsorption of ions is continuous, characteristic of a single phase. Region II is the low-temperature ($b < b_c$), low salt (below L_1 line) regime, Region III is the high-temperature ($b > b_c$), high salt (above the L_1 line) regime, and Region V is the low-temperature

($b < b_c$), high salt (above L_1 and L_2 lines) regime. These regions are the two-phase regions, where the adsorption of ions undergoes an abrupt change at a particular surface charge density, exhibiting a first-order phase transition. Region IV, the low-temperature ($b < b_c$), intermediate salt (above L_1 line but below L_2 line) regime, is a three-phase region, where the adsorption undergoes two closely packed first-order phase transitions. All of these regions (I–V) are bounded by either a first-order line (L_1 and L_2 lines), or a line of critical points, labeled as b_c. It begins at point $C \equiv (0.0056, 0)$ and ends at E $\equiv (0.0064, 5.9)$, separating Regions I and II, below L_1 line, and Regions III and IV, above L_1 line. Another first-order line, L_2 line, separates Region IV and Region V, and it ends together with b_c line at a critical endpoint E.

Regions I and II: below the L_1 line are the two regions that represent the low salt regimes. One aspect of the adsorption in such a regime is the fact that due to low salt concentrations only the counterions participate in the adsorption, because there is simply not too many co-ions around. Indeed, solutions to eqs. (42) and (43) in these regions confirm that $\tau \approx \theta$, which means that $n_{a+} \gg n_{a-}$. This makes sense physically because only the counterions are attracted to the surface. Consequently, the behaviors of τ in these two regions are similar to the behaviors of that in counterion-only case, as discussed in ref. [48].

At high temperature, *i.e.*, $b > b_c$ (Region I), we have a supercritical region where the adsorption is continuous, similar to the prediction from the mean-field theory (see fig. 7 (top)). However, as shown in fig. 7 (top), the shape of the curve (representing the charge regulation parameter τ as a function of g at one loop) resembles a sigmoidal curve, which is qualitatively different from the corresponding mean-field curve. At low surface charge, the number of ions (mainly counterions) adsorbed to the surface, though small, is always greater, if only slightly, than that predicted by the mean-field theory. Thus, correlation effects always facilitate ion adsorption. This is to be expected since an ion (regardless of its sign) gains correlation energy, as manifested in the effective binding energy in eq. (32). As the surface charge increases, the charge regulation parameter τ increases very rapidly within a narrow range of surface charges, indicating a sudden adsorption of large number of ions as can be seen from fig. 7 (top). Note that in this range of surface charges, there are a lot more ions adsorbed than that predicted from the mean-field theory ($\tau > \tau_{\rm MF}$). Finally, as the surface charge further increases, τ slowly approaches its asymptotic value and saturates near $\tau \approx 1$.

This behavior of the charge regulation parameter as a function of surface charge suggests that correlation effects give rise to a kind of cooperativity in the adsorption process [52, 53]. Physically, it can be attributed to the fact that the adsorbed ions facilitate adsorption of other ions in their neighborhood. At low surface charge, the ions are adsorbed mainly through the attraction between the negatively charged surface and positively charged counterions and the interaction between the adsorbed ions and counterions is negligible. As the surface charge increases, more counterions are adsorbed to the surface and the effective

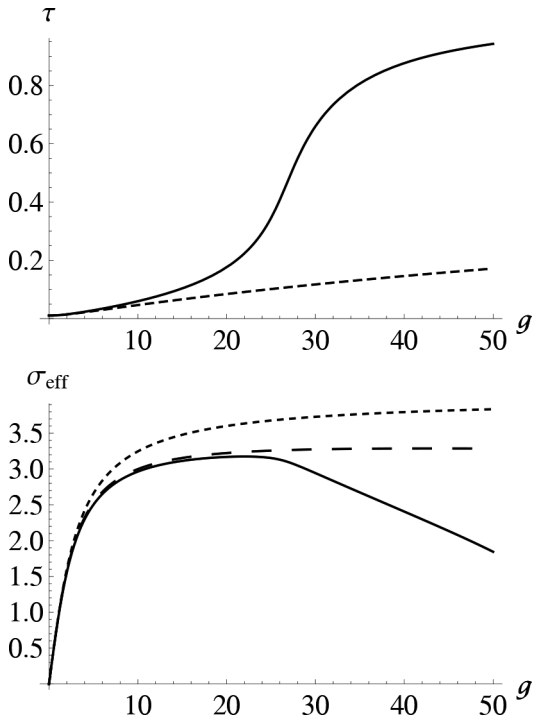

Fig. 7. Top: the charge regulation parameter τ as a function of g in Region I (high temperature, low salt) with $b = 0.01$ and $\kappa\ell_B = 2.1$. The dashed line is the prediction from the mean-field theory given by eq. (37). In contrast to the mean-field prediction, the behavior of τ resembles a sigmoidal curve, suggesting that correlation effects give rise to cooperative behaviors in the adsorption of ions. Bottom: a plot of the one-loop effective charge, $\sigma_{\rm eff}$, given by eq. (A.20), as a function of g. The dotted line is the mean-field theory without charge regulation. The dashed line is one-loop $\sigma_{\rm eff}$ without charge regulation. As can be seen, correlation effects on charge regulation can be drastic: the effective charge $\sigma_{\rm eff}$ decreases substantially as surface charge increases ($g \approx 30$), where cooperative adsorption occurs. Thus, correlation effects enhance the adsorption of the counterions to the point where they effectively renormalize the surface charge density towards zero. Hence, the effective charge is reduced drastically.

binding energy $\mathcal{G}(0,0)$ of the ions arising from the adsorbed ions is not negligible. This attractive interaction enhances the adsorption of the ions and leads to the cooperative adsorption since $\mathcal{G}(0,0)$ depends on τ and θ. The saturation of τ (near $\tau \approx 1$) is caused by the fact that the surface is now effectively neutral and the ions are no longer attracted to the surface. It is important to note that, for $(1,1)$ electrolyte, the charge regulation parameter, though close to it, never exceeds one. This indicates that symmetric electrolyte cannot reverse the sign of the charge density of the surface.

In order to gain further physical insights, let us discuss the one-loop electrostatic potential $\varphi_1(z)$ for symmetric electrolyte as calculated in appendix A.2. Even with correlation effects and charge regulation included, $\varphi_1(z)$ decays exponentially at large distance, $\varphi_1(z) \sim \sigma_{\rm eff}\, e^{-\kappa|z|}$, as in the mean-field theory, but with an effective charge

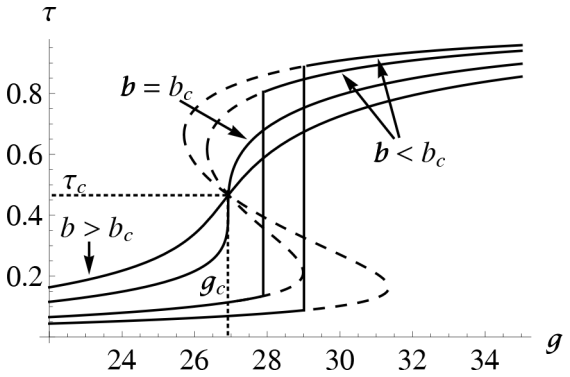

Fig. 8. The charge regulation parameter τ as a function of g in Region I (high temperature, low salt) with $b = 0.0075$, and Region II (low temperature, low salt) with $b = 0.0035$ and $b = 0.0025$, passing through the critical point, $b_c = 0.0056$, below L_1 line with $\kappa\ell_B = 0.05$. Starting from Region I, where $b > b_c$, the ion adsorption is continuous. As the temperature is lowered, the slope in the sigmoidal curve increases; at $b = b_c$, the slope becomes infinite and the adsorption of ions undergoes a second-order phase transition; and as the temperature decreases further ($b < b_c$), ion adsorption becomes discontinuous in Region II. Thus, the three cases, $b > b_c$, $b = b_c$ and $b < b_c$, represent supercritical (Region I), critical (on the b_c line), and two-phase coexistence (Region II), respectively. The dashed lines represent the unstable solutions of τ where the surface free energy of the system is a minimum, but not a globally minimum.

given by eq. (A.20), instead of eq. (38), see also fig. 3. As depicted in fig. 7 (bottom), we observe that for low surface charge density, the values of σ_{eff} at one loop (with or without charge regulation) are close to the mean-field value, as expected. However, as the surface charge increases, the one-loop σ_{eff} without charge regulation deviates somewhat from the mean-field prediction, but with charge regulation, the behavior of σ_{eff} is drastically altered to the point where σ_{eff} now heads towards zero with increasing surface charge, indicating an effective neutralization of the surface charge by the adsorbed ions.

As the temperature reduces, or as b decreases, the slope of the sigmoidal curve representing the charge regulation parameter τ as a function of g increases (see fig. 8). When b reaches a critical value b_c, the slope becomes infinite and the adsorption of ions undergoes a second-order phase transition. In our example, depicted in fig. 8, the second-order transition occurs at $b_c \approx 0.0056$ and $g_c \approx 27$ for $\kappa\ell_B = 0.05$, with $\tau_c \approx 0.46$. Thus, at this critical point, about 46% of the $n_0 \approx 0.36\,\text{nm}^{-2}$ surface charge has been neutralized at a temperature of 250 K in a 10^{-6} M salt solution, consisting of ions with a diameter of 0.7 Å. This suggests that phase transitions may not occur for monovalent counterions at room temperature under physiological conditions.

As the temperature decreases further, *i.e.*, $b < b_c$, we reach the two-phase region (Region II), where within a certain range of g, we have two stable solutions to eqs. (42) and (43), and the adsorption of ions undergoes a first-order phase transition at a certain g within that range (see fig. 8). It is characterized by a jump discontinuity in the charge regulation parameter, indicating a large fraction of ions is adsorbed abruptly ($\sim 80\%$) to the surface. (The precise value of g at which the jump occurs is determined by the two stable solutions having the same free energy.) These behaviors in the adsorption processes, exhibiting supercritical, critical, and a first-order phase transition, are similar to those of a liquid-gas transition [32]. Note that similar adsorption behaviors are predicted also in the Langmuir adsorption model with short-ranged attractive interactions between the adsorbed particles [50]. Lastly, we remark that the quantitative value of τ (at a particular g) depends also on $\kappa\ell_B$, but as long as the system parameters are below the L_1 line, the qualitative features of the adsorption process remains intact.

Regions III, IV, and V: representing the high salt regime (above L_1 line), the common characteristics in these regions are that i) there are always multiple solutions to eqs. (42) and (43), and ii) one of the solutions is always $\tau \approx 1$. The solution $\tau \approx 1$ represents, physically, a surface whose surface charge is effectively neutralized by the adsorbed ions. Clearly, the system must have enough counterions to accomplish this, and above L_1 line, there is enough of added salt that provides an excess amount of mobile ions to make the $\tau \approx 1$ solution possible. In addition, the values of the coverage θ corresponding to the $\tau \approx 1$ solution are such that $\theta \gg \tau$, indicating that a substantial amount of co-ions is also adsorbed onto the surface. This makes sense physically because at $\tau \approx 1$ the surface charge has been almost neutralized. Therefore, the repulsion between the surface and the co-ions is substantially reduced, leading to adsorption of the co-ions as facilitated by correlation effects. As depicted, respectively, in figs. 9 and 10 (bottom), Regions III and V are the two-phase regions, where a first-order phase transition occurs, and in fig. 10 (top), Region IV is the three-phase region, where two closely packed first-order phase transitions take place.

In Region III, the high temperature ($b > b_c$), high salt (above L_1 line) regime, the behavior of charge regulation parameter τ for small g is similar to that of Region I, see fig. 9 (top). But, for large g, when τ gets close to $\tau \geq 0.5$, it displays a finite jump discontinuity to the solution $\tau \approx 1$ and the adsorption proceeds through a first-order phase transition. Unlike the first-order phase transition occurred in Region II, the magnitude of the jump in Region III is significantly smaller. In our example, in fig. 9 (top), τ jumps from $\tau \approx 0.8$ to $\tau \approx 1$ at $g \approx 32$. This jump in adsorption is caused by a large excess amount of mobile ions in the system because of higher salt concentration. Indeed, the magnitude of the jump depends on the salt concentration. In particular, when the system parameters are below l_1 line, the jump is small because the $\tau \approx 1$ solution exists only for sufficiently large g. When the system parameters are above l_1 line, the $\tau \approx 1$ solution exists even for $g \to 0$ and the magnitude of the jump becomes greater, as depicted in fig. 9 (bottom). As the temperature is lowered in Region III, we reach the b_c line, where the adsorption of ions undergoes a second-order phase transition, similar to the one at the b_c line between Region I and Region II. However, in

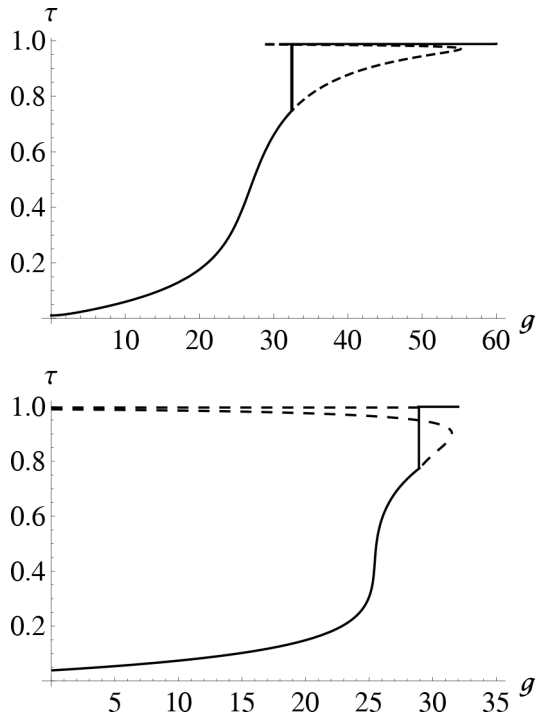

Fig. 9. The charge regulation parameter τ as a function of g in Region III (high temperature, high salt) with $b = 0.01$ and $\kappa\ell_B = 2.15$ (below the l_1 line) (top) and $\kappa\ell_B = 3$ (above the l_1 line) (bottom). Note the existence of the $\tau \approx 1$ solution, which is a common characteristic for Region III, IV, and V, occurs at a finite g ($g \approx 27$ in this example) below l_1 line, and $g = 0$, above l_1 line. At $g \approx 32$ (top) and $g \approx 27$ (bottom), τ displays a finite jump from $\tau \approx 0.8$ to $\tau \approx 1$, and $\tau \approx 0.6$ to $\tau \approx 1$, respectively. These jumps are smaller in magnitude than the jump in Region II. But as $\kappa\ell_B$ increases further, the gap between the unstable solutions (dashed lines) and the $\tau \approx 1$ solution widens. Consequently, the magnitude of jump becomes greater as salt concentration increases.

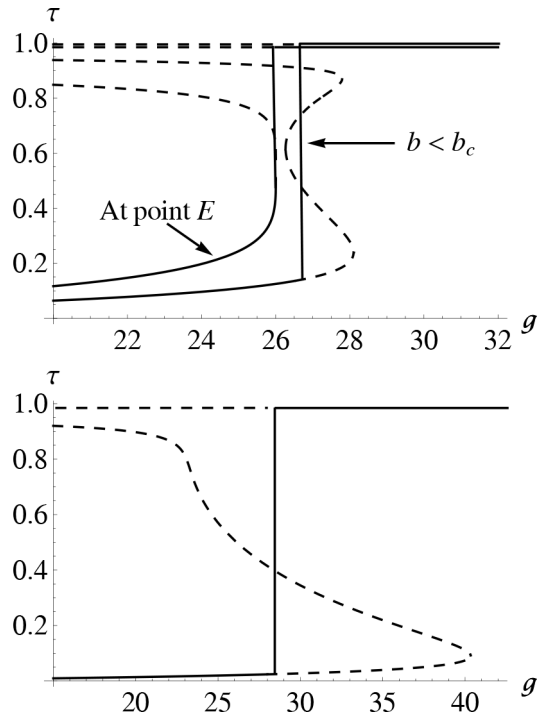

Fig. 10. The charge regulation parameter τ as a function of g in Region IV (low temperature, intermediate salt) with $b = 0.004$ and $\kappa\ell_B = 3$, and at the critical endpoint E $= (0.0064, 5.9)$ (top), and in Region V (low temperature, high salt) with $b = 0.001$ and $\kappa\ell_B = 3$ (bottom). In Region IV, the adsorption of ions undergoes two closely packed first-order phase transitions: τ jumps from $\tau \approx 0.15$ to $\tau \approx 0.7$, and immediately to $\tau \approx 1$, all at $g \approx 27$. Therefore, Region IV represents the coexistence of three phases. At the critical endpoint, E, the adsorption does not undergo a second-order phase transition. Instead, τ displays a finite jump, as one of the stable solutions ($\tau \approx 0.7$) disappears. In Region V, the adsorption of ions undergoes a first-order phase transition, $\tau \approx 0$ to $\tau \approx 1$ at $g \approx 28$. Note the magnitude of the jump.

the regions above the L_1 line, the charge regulation parameter τ also displays a finite jump, at a large g, to the $\tau \approx 1$ solution, characteristic of Region III (see fig. 9).

In Region IV, the low-temperature ($b < b_c$), intermediate salt (above L_1 line but below L_2 line) regime, we observe that the charge regulation parameter τ for small g and for large g behaves similarly to that of Region II and of Region III, respectively. Thus, the adsorption of ions proceeds through two closely packed first-order phase transitions. In our example, in fig. 10 (top), τ jumps from 0.15 to 0.7, and immediately to $\tau \approx 1$ at $g \approx 27$. Therefore, Region IV represents the coexistence of three phases ($\tau \approx 0.15$, $\tau \approx 0.7$, and $\tau \approx 1$ at $g \approx 27$, in our example), similar to the gas-liquid-solid coexistence at the triple point. When the system parameters are near the critical endpoint E, where L_2 line and b_c line end together, the adsorption does not undergo a second-order phase transition. Instead, τ displays a finite jump, as one of the stable solutions ($\tau \approx 0.7$) disappears, as shown in fig. 10 (top).

In Region V, the low-temperature ($b < b_c$), high salt (above L_2) regime, we observe a first-order phase transition, and the magnitude of the jump in charge regulation parameter τ is large: When the surface charge density is low, only a small number of ions is adsorbed to the surface ($\tau \approx 0$), but when the surface charge density becomes sufficiently high, a large number of ions is adsorbed immediately to the surface ($\tau \approx 1$), via a first-order phase transition, see fig. 10 (bottom). This behavior is similar to a gas condensing directly to the solid phase bypassing the liquid phase, opposite to the sublimation.

4.2 Phase diagram for asymmetric (2, 1) electrolyte

Figure 11 depicts the phase diagram for (2, 1) electrolyte projected onto the $\kappa\ell_B$-b plane. This diagram is divided into six regions. In contrast to the (1, 1) electrolyte case discussed in the previous section, we now have two second-order lines, b_{c1} and b_{c2}, intertwined making Regions II, III, and IV and one first-order line L_1, separating Regions V and VI. The b_{c1} line starts at $(0, 0)$ and b_{c2} at $(0.022, 0)$, and they intersect twice at points A $= (0.025, 1.68)$ and

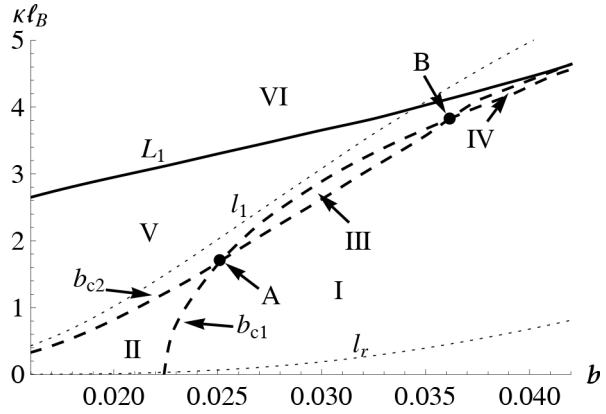

Fig. 11. Phase diagram for asymmetric $(2,1)$ electrolyte in the $(\kappa\ell_B, b)$-plane. It is divided into six regions. Region I is the single phase region, Region II, III, IV, and VI are the two-phase regions, and Region V is the three-phase region. Two second-order lines, the b_{c1} and b_{c2} lines intertwine together, delineating Regions II, III, and IV; they interact at point A $= (0.025, 1.68)$ and B $= (0.036, 3.82)$. A first-order line, L_1 line, separates the intermediate salt region (Region V) from the high salt region (Region VI). In Regions I and II, the l_r line denotes the boundary where charge reversal ($\tau > 1$) occurs. Above l_r line, the charge regulation parameter τ saturates to a value $\tau > 1$ as the surface charge becomes increasingly high. Below l_r line, τ saturates to a value $\tau < 1$. The l_1 line, in Regions V and VI, delineates the existence of a state with $\tau \approx 2$ in the limit as the surface charge vanishes. Below the l_1 line, a state with $\tau \approx 2$ exists at a finite high g. Above the l_1 line, it exists even when $g \to 0$.

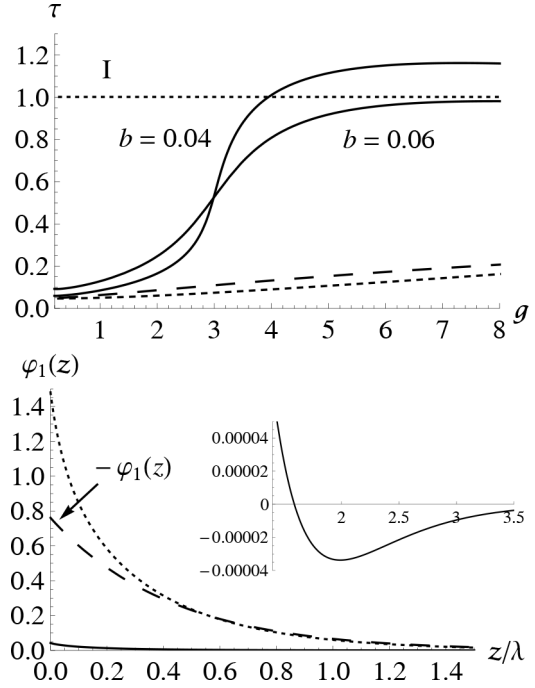

Fig. 12. Top: the charge regulation parameter τ as a function of g with $\kappa\ell_B = 2.4$ for two cases $b = 0.04$, and 0.06 for the asymmetric electrolyte, $p = 2$. The dotted line is the prediction from mean-field theory for the asymmetric $(2,1)$ electrolyte and the dashed line is the one-loop prediction for symmetric $(1,1)$ electrolyte with $b = 0.04$. Bottom: a plot of the one-loop electrostatic potential $\varphi_1(z)$ as a function of z/λ, with $g = 6$, $\kappa\ell_B = 2.4$, and $b = 0.04$ [solid line], and 0.06 [dashed line], for $p = 2$. The dotted line is the one-loop electrostatic potential without charge regulation. For $b = 0.04$, $\tau > 1$ (see top figure) for larger g, so the surface becomes positively charged surface hence $\varphi_1(z) < 0$. For $b = 0.06$, τ is always less than one, which means the charge inversion is not achieved, but the net charge on the surface is sufficiently reduced so that $\varphi_1(z)$ is very small, and even becomes negative for sufficiently large distance (see inset).

B $= (0.036, 3.82)$. The b_{c1}, b_{c2}, and L_1 lines converge asymptotically towards each other at high temperature. Region I, the single-phase region, is the high-temperature ($b > b_{c1}$), low salt (below b_{c2} line) regime, where the adsorption of ions is continuous. Region II is the low-temperature ($b < b_{c1}$), low salt (below b_{c2} line) regime, Region III is the intermediate-temperature ($0.025 < b < 0.036$), intermediate salt (above b_{c2} but below b_{c1}) regime, and Region IV is the high-temperature ($b > 0.036$), intermediate salt (above b_{c1} but below b_{c2}) regime. These regions are the two-phase regions, where the adsorption exhibits a first-order phase transition at a particular value of g. Region V is the intermediate salt (above b_{c1} and b_{c2} lines but below L_1) regime, where the adsorption of ions undergoes two successive first-order phase transitions. Region VI, the high-salt (above L_1 line) regime, is another two-phase region.

Region I: representing the high-temperature and low salt regime, this region is the single-phase region, where the adsorption of ions (divalent counterions and monovalent co-ions) is continuous. Similar to Region I of $(1,1)$ electrolyte, the charge regulation parameter τ as a function of surface charge exhibits a sigmoidal shape, as displayed in fig. 12 (top), indicating the adsorption is cooperative at one loop for $(2,1)$ electrolyte as well. However, there are two crucial differences that distinguish the $(2,1)$ electrolyte from the $(1,1)$ electrolyte. First, the range of g, where the cooperative adsorption occurs, is significantly lower for $(2,1)$ electrolyte. For example, the rapid rise in τ occurs in the range of $1 < g < 4$, for $(2,1)$ electrolyte, but in the range of $10 < g < 30$, for $(1,1)$ electrolyte. This is because the value of g, that produces the same effect in a system with $(1,1)$ electrolyte, g_1, and in a system with $(p,1)$ electrolyte, g_p, is related by $g_1 = p^3 g_p$. Therefore, we expect that $g_2 \approx g_1/8$, which is roughly observed. More importantly, for $(2,1)$ electrolyte, the charge regulation parameter τ can exceed one for sufficiently high salt concentration and high surface charge (see fig. 12 (top)). This ($\tau > 1$) means that adsorbed ions overcompensate the surface charge, so that the sign of the surface charge is reversed. This phenomenon is known as charge reversal [7]. It occurs above the l_r line in the phase diagram of fig. 11 within Region I at sufficiently large surface charge. Below l_r line, τ never become greater than one because of the low salt condition, as there are not enough ions to be adsorbed to overcompensate the surface charge.

Indeed, in the limit of no added salt, the number of counterions times the valency must equal to the number of

charges on the surface, due to charge neutrality. Therefore, even when all the counterions are adsorbed, the surface is, at best, neutral. This is true regardless of the valency of counterions. However, when there is enough of added salt, the charged surface may draw in, due to correlation effects, more than enough counterions (of which there is now an excess amount) to be adsorbed on it so as to overcompensate its surface charge. While correlation has the same effects of drawing counterions close to the surface, there are two fundamental differences between $(1,1)$ and $(2,1)$ electrolytes. First, as we mentioned above, correlation effects are about 8 times greater for divalent counterions than they are for monovalent counterions, under the same condition of temperature, salt concentration, and surface charge. Secondly, the entropy loss due to confinement of the same amount of charge to the surface is a lot more for monovalent than it is for divalent counterions. Therefore, divalent counterions must be more efficient in screening the charged surface, and so under some conditions, charge reversal occurs for divalent but not for monovalent counterions. Note that the amount of added salt required to produce the charge reversal state roughly bears an inverse relationship with temperature, as expected.

In order to gain more insights into charge reversal, we discuss the one-loop electrostatic potential $\varphi_1(z)$ for $(2,1)$ electrolyte as calculated in appendix A.2. Unlike the $(1,1)$ electrolyte, the asymptotic behavior of the one-loop corrections to the electrostatic potential of $(2,1)$ electrolyte is $\langle[\imath\Delta\psi(z)]\rangle_1 \sim -\kappa|z|\,e^{-\kappa|z|}$, for large z, even when charge regulation is switched off. Since the mean-field potential at large distances behaves like $\varphi_0(z) \sim e^{-\kappa|z|}$, $\langle[\imath\Delta\psi(z)]\rangle_1$ dominates $\varphi_0(z)$ for sufficiently large z, and hence, the one-loop electrostatic potential, $\varphi_1(z) = \varphi_0(z)+\langle[\imath\Delta\psi(z)]\rangle_1$, becomes negative for sufficiently large distance. Thus, correlation effects give rise to overscreening of the charged plane by divalent counterions, even with charge regulation switched off. Note that this does not happen for $(1,1)$ electrolyte because monovalent counterions are not efficient at screening compared to divalent counterions. Therefore, overscreening translates to charge reversal when divalent counterions are allowed to be adsorbed. In fig. 12 (bottom), we plot the one-loop electrostatic potential as a function of distance for the two cases where the system parameters are above and below l_r line. Above the l_r line, when $\tau > 1$, the one-loop electrostatic potential is negative, because the surface becomes a positively charged surface. Below l_r line, even though $\tau < 1$, the electrostatic potential is negative for sufficiently large distance (see inset of fig. 12 (bottom)), a distinct characteristic feature of $(2,1)$ electrolyte.

Regions II, III, and IV: These regions are the two-phase regions, that represent the low-temperature, low salt regime (Region II), the intermediate-temperature, intermediate salt regime (Region III), and the high-temperature, intermediate salt regime (Region IV), where the adsorption of ions undergoes a first-order phase transition at a particular g.

From low salt (below the b_{c1} and b_{c2} lines), in Region I, as the temperature decreases, the ion adsorption undergoes a second-order phase transition at $b_{c1} = 0.024$ (for $\kappa\ell_B = 1$), $g_c \approx 3.3$ with $\tau_c \approx 0.5$ (low critical point). This behavior is similar to $(1,1)$ electrolyte. But, unlike the $(1,1)$ electrolyte, the transition for $(2,1)$ electrolyte occurs at $g_c \approx 3.3$ and $b_{c1} \approx 0.024$, which corresponds to a surface charge density of $n_0 \approx 0.15\,\mathrm{nm}^{-2}$ at a temperature of about 300 K in a 0.48 mM salt solution, consisting of ions with a diameter of 2 Å. Therefore, for $(2,1)$ electrolyte, the phase transition, which occurs at room temperature, may be observed experimentally. As temperature decreases further, we reach Region II, where the adsorption of ions undergoes a first-order phase transition near the low critical point (see fig. 13). These behaviors in the charge regulation parameter are similar to a liquid-gas transition, which also occur for $(1,1)$ electrolyte albeit at a much lower temperature.

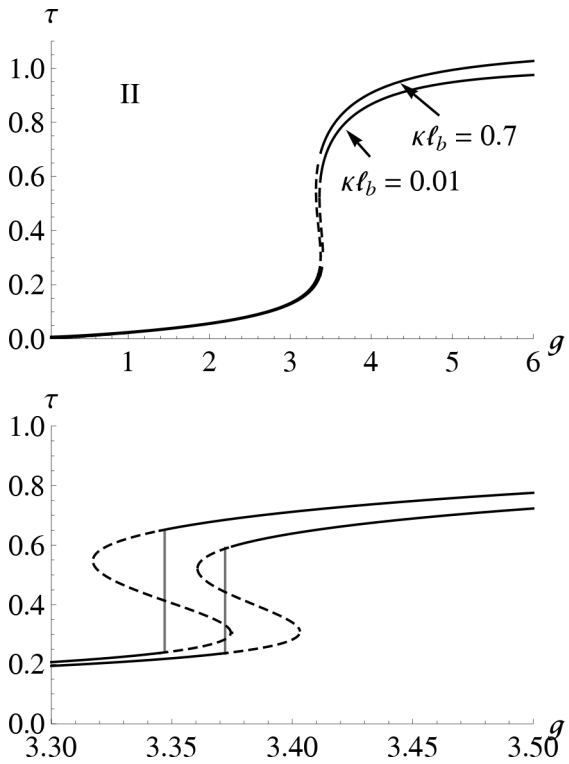

Fig. 13. The charge regulation parameter τ as a function of g in Region II (low temperature, low salt) with $b = 0.02$ and $\kappa\ell_B = 0.01$ and 0.7 (top). The first case ($\kappa\ell_B = 0.01$) represents typical behaviors of τ below the l_r line in Region II, where $\tau < 1$. The second case ($\kappa\ell_B = 0.7$) represents behaviors of τ above the l_r line, where $\tau > 1$, for sufficiently large g. In both cases, the adsorption of ions undergoes a first-order phase transition, in which τ jumps from $\tau \approx 0.2$ to $\tau \approx 0.6$ (bottom).

From intermediate temperature ($0.025 < b < 0.036$), in Region I, as the salt concentration increases, the adsorption of ions undergoes a second-order phase transition at $b_{c2} \approx 0.03$ (for $\kappa\ell_B = 2$), $g_c \approx 4.3$ with $\tau_c \approx 1.6$ (high critical point). The system parameters for this critical point correspond to a surface charge density of $n_0 \approx 0.3\,\mathrm{nm}^{-2}$ at a temperature of about 300 K in a 1.3 mM salt solution, consisting of ions with a diameter of 2.8 Å. As the salt concentration increases further, we reach Region III,

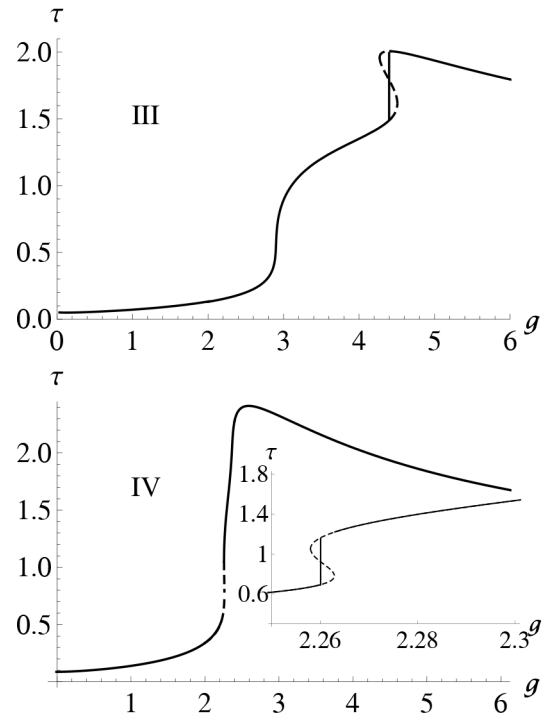

Fig. 14. The charge regulation parameter τ as a function of g in Region III (intermediate temperature, intermediate salt) with $b = 0.03$ and $\kappa\ell_B = 2.7$ (top) and in Region IV (high temperature, intermediate salt) with $b = 0.04$ and $\kappa\ell_B = 4.33$ (bottom). At $g \approx 4.3$ (top) and $g \approx 2.25$ (bottom), τ displays a finite jump from $\tau \approx 1.5$ to $\tau \approx 2$, and from $\tau \approx 0.6$ to $\tau \approx 1.2$, respectively. Note that in Region IV, the transition takes the charged surface to its charge reversal state, see inset (bottom). Note also that τ can reach as high as $\tau \approx 2$, followed by a turning point at which τ starts to decreases as the surface charge increases, exhibiting a reentrant behavior.

where the ion adsorption undergoes a first-order phase transition near the high critical point, see fig. 14 (top). This behavior is similar to the small jump displayed by the charge regulation parameter τ in Region III of $(1, 1)$ electrolyte (see fig. 9). But unlike the Region III of $(1, 1)$ electrolyte, the transition occurs at $\tau > 1$, where the system is already at the charge reversal state.

From high temperature ($b > 0.036$), in Region I, as the salt concentration increases, the adsorption of ions undergoes a second-order phase transition at $b_{c1} \approx 0.04$ (for $\kappa\ell_B = 4$), $g_c \approx 2.26$ with $\tau_c \approx 0.7$ (low critical point). The system parameters for this critical point correspond to a surface charge density of $n_0 \approx 0.5\,\mathrm{nm}^{-2}$ at a temperature of about 300 K in a 3.8 mM salt solution, consisting of ions with a diameter of 4 Å. As the salt concentration increases further, we reach Region IV, where the adsorption of ions undergoes a first-order transition, see fig. 14 (bottom). But, unlike the first-order transitions in Regions II and III, this first-order transition takes the system directly to the charge reversal state, as τ jumps from $\tau \approx 0.6$ to $\tau \approx 1.4$.

In contrast to Region II, the charge regulation parameter τ in Regions III and IV can reach as high as $\tau \approx 2$ near the transition. Moreover, the charge regulation parameter τ reaches a turning point at its maximum, after which it decreases as the surface charge increases further (see fig. 14). Thus, in these regions, the adsorption of ions exhibits a reentrant behavior, which is caused by desorption of ions. Indeed, when $\tau \approx 2$, the surface charge is now positive with a magnitude roughly the same as the original one. Therefore, there is a strong repulsion between the surface and counterions, leading to desorption of ions. Note also that as the surface charge further increases, the charge regulation parameter slowly decays towards $\tau \approx 1$, indicating the surface is becoming neutral.

Regions V and VI: representing the intermediate salt (above b_{c1} and b_{c2} lines but below L_1 line) regime, the charge regulation parameter, in Region V, displays two successive first-order phase transitions (see fig. 15); and representing the high salt (above L_1 line) regime, Region VI is a two-phase region, where the charge regulation parameter undergoes a first-order phase transition (see fig. 16). However, there are a few common characteristics for the two regions: i) The existence of a solution with $\tau \approx 5$–10 and higher, similar to that (but not in magnitude) of Regions III, IV, and V of $(1, 1)$ electrolyte. In particular, the existence of this solution occurs at a finite surface charge, below the l_1 line (in fig. 11) but occurs in the limit when surface charge vanishes, above the l_1 line. This feature is reminiscent of that in Region III of $(1, 1)$ electrolyte. ii) In contrast to $(1, 1)$ electrolyte, the charge regulation parameter exhibits a reentrant behavior in Regions V and VI, similar to Regions III and IV of $(2, 1)$ electrolyte.

Region V can be reached in 3 ways. i) From low temperature ($b < 0.025$), in Region II, as the salt concentration increases, the adsorption of ions undergoes a second-order phase transition at $b_{c2} \approx 0.02$ (for $\kappa\ell_B \approx 1$), $g_c \approx 8$, with $\tau_c \approx 1.5$ (high critical point). The system parameters at this critical point corresponds to $n_0 \approx 0.35\,\mathrm{nm}^{-2}$ at a temperature of 300 K in a 0.38 mM salt solution, consisting of ions with a diameter of 1.8 Å. As the salt concentration increases further, we reach Region V, where the adsorption of ions undergoes a first-order phase transition near the high critical point, in addition to the first-order phase transition occurred near the low critical point in Region II (see fig. 15). ii) From intermediate temperature ($0.025 < b < 0.036$) in Region III, as the temperature decreases or salt concentration increases, the adsorption of ions undergoes a second-order phase transition at $b_{c1} \approx 0.03$ (for $\kappa\ell_B = 3$), $g_c \approx 3$ with $\tau_c \approx 0.5$ (low critical point). The system parameters at this critical point correspond to $n_0 \approx 0.25\,\mathrm{nm}^{-2}$ at a temperature of 300 K in a 2.8 mM salt solution, consisting of ions with a diameter of 2.8 Å. As the salt concentration increases further, we reach Region V, where the adsorption of ions undergoes an additional first-order phase transition near the low critical point (see fig. 15). iii) From high temperature ($b > 0.036$) in Region IV, as the temperature decreases, the adsorption of ions undergoes a second-order phase transition at $b_{c2} \approx 0.038$ (for $\kappa\ell_B = 4$), $g_c \approx 4$ with $\tau \approx 1.5$ (high critical point). The system parameters at this critical point correspond to $n_0 \approx 0.5\,\mathrm{nm}^{-2}$ at a temperature of 300 K in

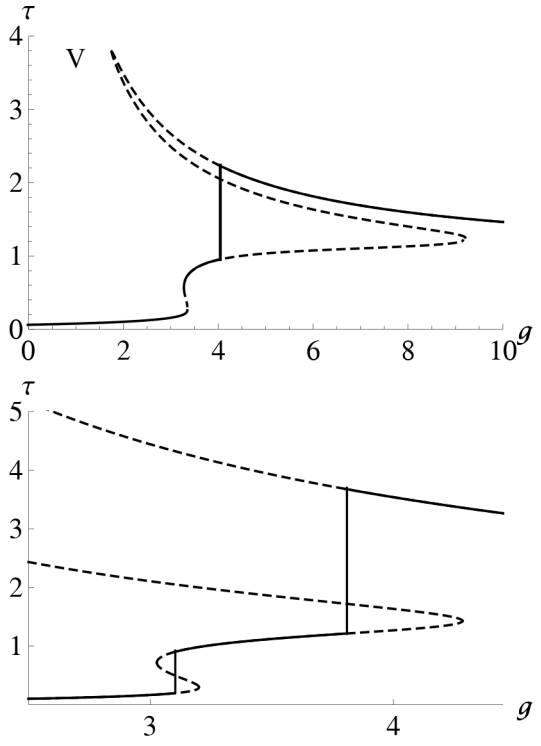

Fig. 15. The charge regulation parameter τ as a function of g in Region V (intermediate salt) with $b = 0.02$ and $\kappa\ell_B = 2$ (below l_1 line) (top) and $\kappa\ell_B = 1$ (above l_1 line) (bottom). Note the existence of the $\tau > 1$ solution, which occurs at finite g ($g \approx 1.5$ in this example), below l_1 line, and $g = 0$, above l_1 line. The adsorption of ions undergoes two first-order phase transitions; the first one takes place at $g \approx 3.3$ (top) and $g \approx 3.1$ (bottom), in which τ jumps, respectively, from $\tau \approx 0.2$ to $\tau \approx 0.6$ and $\tau \approx 0.2$ to $\tau \approx 1$ (near the low critical point); the second one takes place at $g \approx 4$ (top) and $g \approx 3.7$ (bottom) in which τ jumps, respectively, from $\tau \approx 1.2$ to $\tau \approx 2.5$ and $\tau \approx 1.8$ to $\tau \approx 4.5$ (near the high critical point). Note that τ exhibits a reentrant behavior in Region V, as in Regions III and IV.

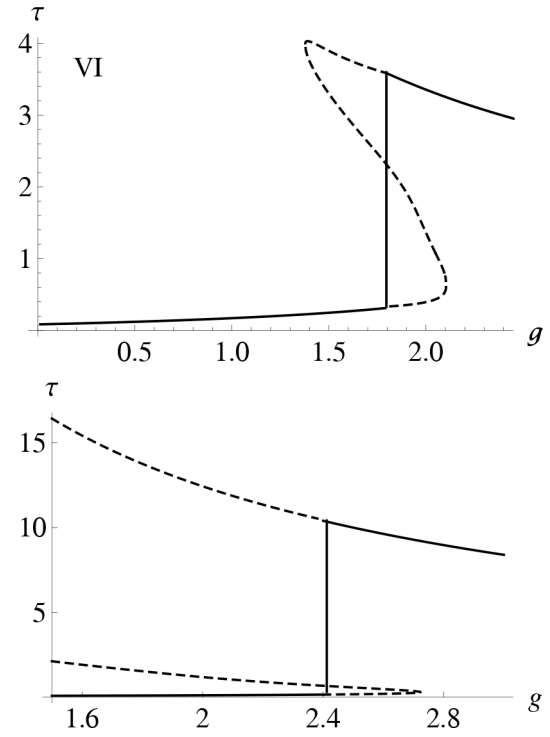

Fig. 16. The charge regulation parameter τ as a function of g in Region VI (high salt) with $b = 0.04$ and $\kappa\ell_B = 4.65$ (below l_1 line) (top) and $b = 0.02$ and $\kappa\ell_B = 4$ (above l_1 line) (bottom). At $g \approx 1.8$ (top) and $g \approx 2.4$ (bottom), τ displays a colossal jump from $\tau \approx 0.2$ to $\tau \approx 3.8$ and $\tau \approx 0.2$ to $\tau \approx 12$, respectively. As g further increase, τ exhibits a reentrant behavior. However, we should note that in this region, our one-loop calculation may break down.

a 5.6 mM salt solution, consisting of ions with a diameter of 3.5 Å. As the salt concentration increases further, we reach Region V, where the adsorption of ions undergoes an additional first-order phase transition (near the high critical point, again). Note that similar to Regions III and IV, the charge regulation parameter also exhibits a reentrant behavior in Region V, right after the transition near the high critical point (see fig. 15).

In Region VI, the number of ions adsorbed is very small ($\tau \approx 0$), at low surface charge, but as the surface charge reaches a certain value, a large number of ions is adsorbed spontaneously to the surface, and the charge regulation parameter displays a colossal jump, from $\tau \approx 0.2$ to $\tau \approx 3.5$, below the l_1 line, and $\tau \approx 0$ to $\tau \approx 10$, above the l_1 line (see fig. 16). This behavior is similar to the behavior in Region V of $(1, 1)$ electrolyte, but the magnitude of the jump is very large. It is important to note that having a solution of such a magnitude as $\tau \approx 4 - 10$, is probably unphysical. Therefore, in the regime where this occurs, Regions V and VI, above the l_1 line, which is the high salt and high surface charge regime, *i.e.*, the strong coupling regime, our one-loop calculation must break down.

5 Conclusion

In summary, we have, in this paper, described the rich physics of charge regulation at one loop, where correlation effects are taken into account. In particular, we find various phase transitions exhibited by $(1, 1)$ and $(2, 1)$ electrolytes. These transitions have physical features that are similar to those exhibited not only in a liquid-gas transition (Ising model) but also in a spin-1 lattice gas, a model for condensation and solidification of a simple fluid [54]. Moreover, we find that $(1, 1)$ and $(2, 1)$ electrolytes have distinct phase diagrams, indicating that charge regulation at one loop is, unlike the mean-field theory, no longer universal.

Our work may be extended in a few ways. First, thanks to the generality of our framework, we can perform similar calculations without much difficulty to address the interesting problem of evaluating the pressure between two charged surfaces across an aqueous solution containing either $(1, 1)$ or $(2, 1)$ electrolytes. This will allow us to make

contact with a body of experimental works that measure pressure between charged surfaces and to, perhaps, resolve a long-standing problem of explaining theoretically the long-ranged attractions between similarly charged surfaces across an electrolyte solution. This long-ranged attractions have been observed experimentally. Secondly, with some efforts, we can extend our calculation to $(3,1)$ electrolyte. This is not just an academic exercise because in real systems there is always a possibility of having a finite amount of electrolytes with valency higher than 2. In fact, it is known experimentally that spermidine ions, which have a valency of 3, condense DNA *in vitro*, not divalent nor monovalent ions. To better understand these systems and beyond, it is interesting to have exact results for arbitrary $(p,1)$ electrolyte. Unfortunately, the exact solution to the PB equation for $(p,1)$ electrolyte in planar geometry has not yet been obtained. Our framework for studying correlation effects requires this exact solution. This is a subject for future study.

However, there is a few fundamental questions about this work that needs further scrutiny. First, there is always a possibility that at some point our one-loop calculations break down, especially for the strong coupling regime where the surface charge and salt concentration are high. Indeed, we have seen that for Regions V and VI of $(2,1)$ electrolyte, the charge regulation parameter at high surface charge is unusually large. It would be interesting but challenging to obtain higher loops corrections. Additionally, our theory contains an ultraviolet cut-off, which we take it to be the size of the ion. In order to regulate this divergence properly, we have to include the hardcore interaction between the ions into our field theoretical framework. This may smooth out the logarithmic divergence in the 2d self-energy. Finally, in a related issue, surface charges are discrete in real systems. It is important to address the discreteness of surface charges in ion adsorption, based on, perhaps, the Langmuir model. The resulting problem, however, does not enjoy in-plane translational invariance. This makes even solving the mean-field PB equation difficult.

The authors thank Fyl Pincus for useful discussion.

Author contribution statement

AWCL proposed the research. Both authors were involved in the theoretical calculations and in the preparation of the manuscript.

Appendix A. The Green's function and the one-loop correction to the electrostatic potential

In this appendix, we present some technical details on constructing the Green's function, solving for the one-loop corrections to the electrostatic potential, and computing the one-loop Helmholtz free energy for the system. We will attempt to write most of the mathematical expressions in a form that is valid for both $p=1$ and $p=2$. Otherwise, we will state clearly for what p the expression is intended.

Appendix A.1. Construction of the Green's function

The Green's function is the inverse of the operator $K(\mathbf{x},\mathbf{x}')$ defined in eq. (14) and satisfies the differential equation eq. (20). Since the mean-field solution depends only on z, we Fourier-transform $G(\mathbf{x},\mathbf{x}')$ in the directions parallel to the plane and write

$$G(\mathbf{x},\mathbf{x}') = \int \frac{\mathrm{d}^2\mathbf{q}}{(2\pi)^2} e^{-i\mathbf{q}\cdot(\mathbf{r}-\mathbf{r}')}\, G(z,z';q), \tag{A.1}$$

where $\mathbf{r}$ and $\mathbf{r}'$ are the two-dimensional position vectors in the plane. Substituting eq. (A.1) into eq. (20), we find

$$\left\{-\partial_z^2 + \alpha^2\kappa^2 + \frac{\kappa^2}{1+p}\left[p\, e^{p\varphi_0(z)} + e^{-\varphi_0(z)} - (1+p)\right] + \frac{2}{\lambda_D}\,\delta(z)\right\} G(z,z';q) = \ell_B \delta(z-z'), \tag{A.2}$$

where $\alpha^2 \equiv 1 + q^2/\kappa^2$ and $2/\lambda_D = \ell_B(p^2 n_{a+} + n_{a-})$. To solve eq. (A.2), we divide the space into three-regions, $z<0$, $0<z<z'$, and $z'<z$. Without loss of generality, we assume $z'>0$, and the solution to the case $z'<0$ can be similarly obtained. We write $G(z,z';q)$ as

$$\begin{aligned}
G_>(z,z';q) &= A(z')h_-(z), \quad \text{for } z>z',\\
G_<(z,z';q) &= B(z')h_-(z) + C(z')h_+(z), \quad \text{for } 0<z<z',\\
G_-(z,z';q) &= D(z')h_-(-z), \quad \text{for } -\infty<z<0,
\end{aligned}$$

where $h_\pm(z)$ are the two independent homogeneous solutions, satisfying

$$\left[-\kappa^{-2}\,\partial_z^2 + \alpha^2 - 1 + \frac{p\, e^{p\varphi_0(z)} + e^{-\varphi_0(z)}}{1+p}\right] h_\pm(z) = 0, \tag{A.3}$$

and the coefficients, $A(z')$, $B(z')$, $C(z')$ and $D(z')$, are determined by imposing the following boundary conditions on the Green's function:

$$\begin{aligned}
&G_-(0,z';q) = G_<(0,z';q),\\
&G_<(z',z';q) = G_>(z',z';q),\\
&\partial_z G_<(z,z';q)|_{z=0} - \partial_z G_-(z,z';q)|_{z=0} = \frac{2}{\lambda_D}\, G(0,z';q),\\
&\partial_z G_<(z,z';q)|_{z=z'} = \ell_B + \partial_z G_>(z,z';q)|_{z=z'}.
\end{aligned}$$

The first two conditions ensures that the Green's function is continuous everywhere, and the next two conditions ensures that the derivative of the Green's function is discontinuous at $z=0$ and $z=z'$ as demanded by the delta-functions in eq. (A.2). In particular, the third boundary condition arises from the coulomb gas confined to a 2D surface. The coefficients can be obtained in a straightforward way, albeit with tedious algebra, and their

expressions are not so illuminating to display here. Fortunately, the relevant quantities to study charge regulation depend only on the diagonal part of the Green's function, $G(z,z;q)$, which can be written in a manageable expression

$$G(z,z;q) = \frac{\ell_B}{\mathcal{W}(\alpha)}\left[h_+(z)\,h_-(z) + \mathcal{M}(\alpha)\,h_-^2(z)\right], \quad \text{(A.4)}$$

where $\mathcal{W}(\alpha) \equiv h'_+(z)h_-(z) - h_+(z)h'_-(z)$ is the Wronskian (a prime denotes differentiation with respect to z), and

$$\mathcal{M}(\alpha) \equiv -\frac{1}{2}\left[\frac{h_+(0)}{h_-(0)} + \frac{h'_+(0)}{h'_-(0)}\right] + \frac{\mathcal{W}(\alpha)}{2h'_-(0)[h_-(0) - h'_-(0)\lambda_D]}\,. \quad \text{(A.5)}$$

So far, eq. (A.4) represents a general expression for $G(z,z;q)$ in terms of the homogeneous solutions $h_\pm(z)$, valid for arbitrary p. However, $h_\pm(z)$ can only be solved from eq. (A.3) for $p = 1$ and 2, because those are the cases where exact solutions to the PB equation are known. It turns out that the homogeneous solutions $h_\pm(z)$ can be written in the following form, valid for both $p = 1$ and 2:

$$h_\pm(z) = e^{\pm\alpha\kappa z}\left[1 \mp \frac{f(z)}{\alpha} + \frac{g(z)}{\alpha^2}\right], \quad \text{(A.6)}$$

where $f(z)$ and $g(z)$ can be written separately for $p = 1$ and $p = 2$ as

$$f(z) \equiv \begin{cases} \coth x_1, & \text{for } p = 1, \\ \dfrac{3\sinh x_2 \cosh x_2}{2(\cosh x_2 - 2)(\cosh x_2 + 1)}\,, & \text{for } p = 2, \end{cases} \quad \text{(A.7)}$$

$$g(z) \equiv \begin{cases} 0, & \text{for } p = 1, \\ \dfrac{\cosh x_2 + 1}{2(\cosh x_2 - 2)}\,, & \text{for } p = 2, \end{cases} \quad \text{(A.8)}$$

where $x_p \equiv \kappa(z + z_p)$, $\kappa z_p \equiv -\log\gamma_p$, and γ_p are given by eqs. (35) and (36) for $p = 1$ and $p = 2$, respectively. Using eq. (A.6), it is straightforward to work out the Wronskian

$$\mathcal{W}(\alpha) = \begin{cases} \dfrac{2\kappa}{\alpha}\,(\alpha^2 - 1), & \text{for } p = 1, \\ \dfrac{\kappa}{2\alpha^3}\,(\alpha^2 - 1)\,(4\alpha^2 - 1), & \text{for } p = 2. \end{cases} \quad \text{(A.9)}$$

Similarly, $\mathcal{M}(\alpha)$ can be worked out by substituting eq. (A.6) into eq. (A.5), but their expressions are rather too long to reproduce here. Instead, we list them in appendix B (see eq. (A.2)).

To discuss the self-energy in physical terms, it may be more convenient to split it into three contributions, $G(\mathbf{x},\mathbf{x}) = 2V_0 + G_{\rm DH}(0) + \mathcal{G}(z,z)$, where

$$V_0 \equiv \frac{\ell_B}{2}\int \frac{\mathrm{d}^2\mathbf{q}}{(2\pi)^2}\,\frac{1}{2q}\,,$$

is the bare (infinite) self-energy,

$$G_{\rm DH}(0) \equiv \frac{\ell_B}{2}\int \frac{\mathrm{d}^2\mathbf{q}}{(2\pi)^2}\left(\frac{1}{\sqrt{q^2+\kappa^2}} - \frac{1}{q}\right) = -\frac{\ell_B\kappa}{4\pi}\,,$$

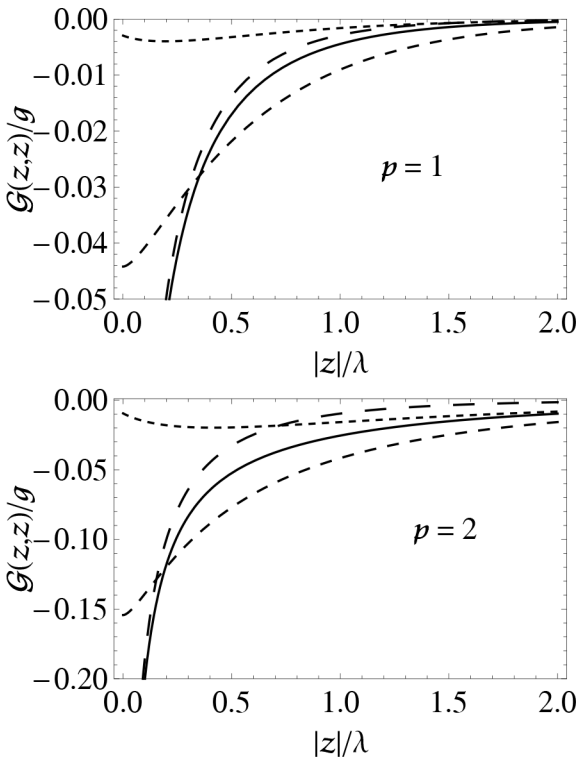

Fig. 17. A plot of $\mathcal{G}(z,z)$ (divided by g) as a function of z/λ (the solid line) for $p = 1$ (top) and $p = 2$ (bottom), with $s = 1$, $\theta = 0.8$, and $\tau = 0.6$. As given in eq. (A.10), $\mathcal{G}(z,z)$ represents the contribution to the self-energy of an ion from the presence of the charged plate along with its counterions and co-ions. It can be written as a sum of two contributions: $\mathcal{G}(z,z) = \mathcal{G}_{2d}(z,z) + \mathcal{G}_{3d}(z,z)$, where $\mathcal{G}_{2d}(z,z)$ (the long-dashed line) is the self-energy of an ion at a distance z away from a surface on which a coulomb gas is confined and it is given by eq. (33). Note that the logarithmic divergence in $\mathcal{G}(z,z)$ as $z \to 0$ stems from $\mathcal{G}_{2d}(z,z)$, since $\mathcal{G}_{3d}(z,z)$ (the dotted line) remains finite as $z \to 0$. The dashed line represents $\mathcal{G}(z,z)$ without charge regulation, *i.e.*, $\theta = \tau = 0$, in which case, $\mathcal{G}(z,z)$ no longer diverges as $z \to 0$.

is the Debye-Huckel self-energy, and

$$\mathcal{G}(z,z) = \int \frac{\mathrm{d}^2\mathbf{q}}{(2\pi)^2}\,\frac{\ell_B}{\mathcal{W}(\alpha)}\left\{h_+(z)h_-(z) - \frac{\mathcal{W}(\alpha)}{2\alpha\kappa} + \mathcal{M}(\alpha)\,h_-^2(z)\right\}, \quad \text{(A.10)}$$

is the self-energy of an ion in the presence of the charged plate at a distance z away from it. In fig. 17, we plot $\mathcal{G}(z,z)$ for both $p = 1$ and $p = 2$. It is clear that for large $|z| \to \infty$, $\mathcal{G}(z,z) \sim -e^{-2\kappa|z|}$ at finite s. On the other hand, in the limit $s \to 0$, we find $\mathcal{G}(z,z) \sim -3\,\ell_B/(8\pi|z|)$, which decays algebraically as $|z| \to \infty$. In both cases, $\mathcal{G}(z,z) \to 0$ as $|z| \to \infty$. Thus, the self-energy of an ion approaches the bulk value, which is given by the Debye-Huckel contribution, as it should be.

Furthermore, it should be noted that $\mathcal{G}(z,z)$ is always negative. This indicates that an ion (regardless of the sign of its charge) gains (correlation) energy as it gets closer to

the plate. In fact, as long as there is charge regulation, *i.e.*, when $\tau \neq 0$ and $\theta \neq 0$, $\mathcal{G}(z,z)$ diverges logarithmically as $|z| \to 0$. This divergence arises from the fluctuations of a Coulomb gas confined to a plane (see fig. 17). Indeed, evaluating $\mathcal{G}(z,z)$ at $z=0$ from eq. (A.10), we can write, after some algebra,

$$\mathcal{G}(0,0) = \int \frac{\mathrm{d}^2\mathbf{q}}{(2\pi)^2} \frac{\ell_B}{2\alpha\kappa} \left\{ -\frac{1}{1+\alpha\kappa\lambda_D} + \frac{\alpha\kappa\lambda_D^2}{1+\alpha\kappa\lambda_D} \left[\frac{h'_-(0)+\alpha\kappa h_-(0)}{h_-(0)-\lambda_D h'_-(0)} \right] \right\}. \quad \text{(A.11)}$$

In this form, which is valid for $p=1$ and 2, $\mathcal{G}(0,0)$ is manifestly written as a sum of two contributions: $\mathcal{G}(0,0) = \mathcal{G}_{2d}(0,0) + \mathcal{G}_{3d}(0,0)$. The first term

$$\mathcal{G}_{2d}(0,0) = -\frac{\ell_B}{2} \int \frac{\mathrm{d}^2\mathbf{q}}{(2\pi)^2} \frac{1}{\alpha\kappa\,(1+\alpha\kappa\lambda_D)},$$

comes from the contribution to the self-energy from the two-dimensional adsorbed ions. It is logarithmically divergent, and we use a, the size of an ion, as a microscopic cut-off to regularize it; this gives

$$\mathcal{G}_{2d}(0,0) \approx -\frac{\ell_B}{4\pi\lambda_D} \left[\ln\left(2\pi\lambda_D/a\right) - \ln\left(1+\kappa\lambda_D\right) \right]. \quad \text{(A.12)}$$

Note, however, that $\mathcal{G}_{2d}(0,0)$ vanishes when $\tau = \theta = 0$, *i.e.*, when there is no adsorbed ions.

The second term in eq. (A.11), $\mathcal{G}_{3d}(0,0)$, may be interpreted as the contribution to the self-energy of an ion located at $z=0$ from the fluctuations of the free ions in the bulk. It can be written in a form that is valid for $p=1$ and $p=2$ as

$$\mathcal{G}_{3d}(0,0) = \frac{\ell_B}{2} \int \frac{\mathrm{d}^2\mathbf{q}}{(2\pi)^2} \left(\frac{1}{\alpha\kappa + 1/\lambda_D} \right) \times \left\{ \frac{\alpha f'(0)+g'(0)}{(\alpha\kappa+1/\lambda_D)[\alpha^2+\alpha f(0)+g(0)]-[\alpha f'(0)+g'(0)]} \right\}, \quad \text{(A.13)}$$

where $f(z)$ and $g(z)$ are given in eqs. (A.8) and (A.9), respectively. An exact but long expression for $\mathcal{G}_{3d}(0,0)$ is presented in appendix B. First, we note that $\mathcal{G}_{3d}(0,0)$ is perfect finite, even in the limit $\lambda_D \to \infty$, *i.e.*, $\tau = \theta = 0$, when there is no ions absorbed onto the surface. This can be seen either from eq. (A.13) or from fig. 17. Thus, the divergence in $\mathcal{G}(0,0)$ disappears when there is no absorbed ions on the plate (see fig. 17). This implies that the nature of the electrostatic correlations is distinct for charged surfaces with or without charge regulation.

Appendix A.2. One-loop corrections to the electrostatic potential

The differential equation for the one-loop corrections to the electrostatic potential, $\langle[\imath\Delta\psi(z)]\rangle_1$, is given by eq. (27)

$$\left\{ -\partial_z^2 + \frac{\kappa^2}{1+p} \left[p\, e^{p\varphi_0(z)} + e^{-\varphi_0(z)} \right] \right\} \langle[\imath\Delta\psi(z)]\rangle_1 = \frac{\kappa^2 \mathcal{G}(z,z)}{2(1+p)} \left[p^2 e^{p\varphi_0(z)} - e^{-\varphi_0(z)} \right],$$

where $\mathcal{G}(z,z)$ is given by eq. (A.10). The two boundary conditions are given by i) $\langle[\imath\Delta\psi(z)]\rangle_1 \to 0$ as $z \to \infty$ and ii) $\partial_z \langle[\imath\Delta\psi(z)]\rangle_1|_{z=0} = 0$. We seek the solution of the form

$$\langle[\imath\Delta\psi(z)]\rangle_1 = \int \frac{\mathrm{d}^2\mathbf{q}}{(2\pi)^2} \frac{\ell_B}{\mathcal{W}(\alpha)} \left[\mathcal{H}_1(z) + \mathcal{M}(\alpha)\, \mathcal{H}_2(z) \right], \quad \text{(A.14)}$$

where $\mathcal{H}_i(z)$ $(i=1,2)$ are the solutions to the inhomogeneous differential equations

$$\left\{ -\partial_z^2 + \frac{\kappa^2}{1+p} \left[p\, e^{p\varphi_0(z)} + e^{-\varphi_0(z)} \right] \right\} \mathcal{H}_i(z) = \kappa^2 \mathcal{F}_i(z), \quad \text{(A.15)}$$

and the functions $\mathcal{F}_1(z)$ and $\mathcal{F}_2(z)$ are defined by (for both $p=1$ and $p=2$),

$$\mathcal{F}_i(z) \equiv \frac{p^2 e^{p\varphi_0(z)} - e^{-\varphi_0(z)}}{2(1+p)} \times \begin{cases} h_+(z)\, h_-(z) - \mathcal{W}(\alpha)/(2\alpha\kappa), & \text{for } i=1, \\ h_-^2(z), & \text{for } i=2. \end{cases}$$

It is straightforward to find the inhomogeneous solutions $\mathcal{H}_i(z)$ and they can be written as

$$\mathcal{H}_i(z) = y_0(z) \left[\mathcal{B}_i(\alpha) + y_i(z) \right], \quad \text{(A.16)}$$

where $y_0(z) \equiv \varphi_0'(z)/\kappa$ is the homogeneous solution to eq. (A.15), $\varphi_0(z)$ is the mean-field potential given by eq. (34),

$$\mathcal{B}_i(\alpha) \equiv -\left. \frac{\partial_z [y_0(z) y_i(z)]}{y_0'(z)} \right|_{z=0}, \quad \text{(A.17)}$$

are constants (the exact expressions for $\mathcal{B}_i(\alpha)$ are presented in appendix B) to ensure that the boundary condition, $\partial_z \mathcal{H}_i(z)|_{z=0} = 0$, is satisfied

$$y_1(z) \equiv \frac{1}{8\alpha^4} \times \begin{cases} -\alpha^2 \coth x_1, & \text{for } p=1, \\ \operatorname{csch} x_2 + \left(\alpha^2 - 1\right)(\kappa z - \coth x_2) \\ \quad - \left(4\alpha^2 - 3\right) \dfrac{\sinh x_2}{\cosh x_2 - 2}, & \text{for } p=2, \end{cases}$$

and

$$y_2(z) \equiv \frac{e^{-2\alpha\kappa z}}{8\alpha} \times \begin{cases} \dfrac{1+\alpha\coth x_1}{\alpha^2}, & \text{for } p=1, \\ \dfrac{t_1(z)}{4\alpha^2-1} + \dfrac{t_2(z)}{\alpha} + \dfrac{t_3(z)}{\alpha^2} + \dfrac{t_4(z)}{\alpha^3} \\ \quad + \dfrac{1}{\alpha^4}, & \text{for } p=2, \end{cases}$$

where

$$t_1(z) \equiv 12(\cosh x_2 + 2\,\alpha \sinh x_2),$$

$$t_2(z) \equiv \frac{8}{3}\coth x_2 + \frac{12\,\mathrm{csch}\, x_2}{\cosh x_2 - 2} + \frac{17(2-\cosh^2 x_2)}{3\sinh x_2},$$

$$t_3(z) \equiv \frac{2\cosh x_2\,(5-\cosh x_2)}{\cosh x_2 - 2},$$

and

$$t_4(z) \equiv \frac{3\sinh x_2}{\cosh x_2 - 2} + \frac{4}{3}\coth\left(\frac{x_2}{2}\right) - \frac{1}{3}\sinh x_2.$$

In the above formulae, we have made use of x_p defined earlier by $x_p \equiv \kappa(z+z_p)$, $\kappa z_p \equiv -\log\gamma_p$, and γ_p are given by eqs. (35) and (36) for $p=1$ and $p=2$, respectively. Note that there is a term proportional to z in $y_1(z)$ for $p=2$. It has important implication for the one-loop electrostatic potential below. Finally, substituting $\mathcal{H}_1(z)$ and $\mathcal{H}_2(z)$ into eq. (A.14), we obtain a complicated expression for $\langle[\imath\Delta\psi(z)]\rangle_1$, especially for $p=2$.

In fig. 18, we plot $\langle[\imath\Delta\psi(z)]\rangle_1$ as a function of z. As expected, $\langle[\imath\Delta\psi(z)]\rangle_1$ seems to decay with distance to zero exponentially. However, it is probably more instructive to disscuss the asymptotics of $\langle[\imath\Delta\psi(z)]\rangle_1$ as $|z|\to\infty$. For $p=1$, we find

$$\langle[\imath\Delta\psi(z)]\rangle_1 = -\frac{\ell_B\kappa}{8\pi}\,\mathcal{A}_1\gamma_1\,e^{-\kappa|z|} + \mathcal{O}(e^{-2\kappa|z|}), \quad \text{(A.18)}$$

where $\mathcal{A}_1$ is given by

$$\mathcal{A}_1 = \int_1^\infty \frac{\mathrm{d}\alpha}{\alpha^2-1}\left\{8\alpha^2\left[\mathcal{B}_1(\alpha) + \mathcal{M}(\alpha)\,\mathcal{B}_2(\alpha)\right] - 1\right\}. \quad \text{(A.19)}$$

Thus, for monovalent counterions we can define an effective charge at one loop

$$\sigma_{\mathrm{eff}}^{(1)} = \sigma_{\mathrm{eff}}^{(0)}\left[1 - \left(\frac{\ell_B\kappa}{8\pi}\right)\mathcal{A}_1\right], \quad \text{(A.20)}$$

where $\sigma_{\mathrm{eff}}^{(0)}$ is the mean-field effective charge given in eq. (38).

For $p=2$, we find

$$\langle[\imath\Delta\psi(z)]\rangle_1 = -\frac{\ell_B\kappa}{8\pi}\left[\mathcal{A}_2 + (3/2)(\log 3)\,\kappa|z|\right]\gamma_2\,e^{-\kappa|z|} + \mathcal{O}(e^{-2\kappa|z|}), \quad \text{(A.21)}$$

where $\mathcal{A}_2$ is given by

$$\mathcal{A}_2 = 24\kappa\int_1^\infty \frac{\alpha\,d\alpha}{\mathcal{W}(\alpha)}\left[\mathcal{B}_1(\alpha) + \mathcal{M}(\alpha)\,\mathcal{B}_2(\alpha) - \frac{5\alpha^2-4}{8\alpha^4}\right]. \quad \text{(A.22)}$$

It is important to observe that for sufficiently large $|z|$, $\langle[\imath\Delta\psi(z)]\rangle_1 \sim -\kappa|z|\,e^{-\kappa|z|}$ dominates even the mean-field electrostatic potential, since $\varphi_0(z)\sim e^{-\kappa|z|}$. Thus, we obtain an interesting result that the one-loop electrostatic potential, $\varphi_1(z) = \varphi_0(z) + \langle[\imath\Delta\psi(z)]\rangle_1$, always becomes negative for sufficiently large z. Physically, this suggests that divalent counterions overscreen the charged plate, so that it appears to be oppositely charged at large distances. While this is the case with or without charge regulation, it is clear when the surface charge is zero, $\varphi_1(z)$ vanishes identically since $\gamma_2 = 0$. However, with charge regulation, we could have a situation where just enough of the divalent counterions are absorbed to neutralize the surface charges, *i.e.*, $\tau = 1$. In this case, we have a neutral surface (hence, the mean-field potential $\varphi_0(z) = 0$), but with a monolayer of a Coulomb gas confined to the surface, whose fluctuations, described by $\mathcal{G}_{2d}(z,z)$ in eq. (33), give rise to a non-zero electrostatic potential given by (for $\tau = 1$)

$$\langle[\imath\Delta\psi(z)]\rangle_1 = -\frac{\kappa\ell_B(p-1)}{8\pi} \times \int_1^\infty \mathrm{d}\alpha\,\frac{2\alpha e^{-\kappa|z|} - e^{-2\alpha\kappa|z|}}{(1+\alpha\kappa\lambda_D)(4\alpha^2-1)}, \quad \text{(A.23)}$$

which decays exponentially for large z, in contrast to eq. (A.21). Note that this result is general, valid for arbitrary p, and in particular, for monovalent counterions ($p=1$), $\langle[\imath\Delta\psi(z)]\rangle_1$ remains zero at $\tau = 1$. Thus, there is

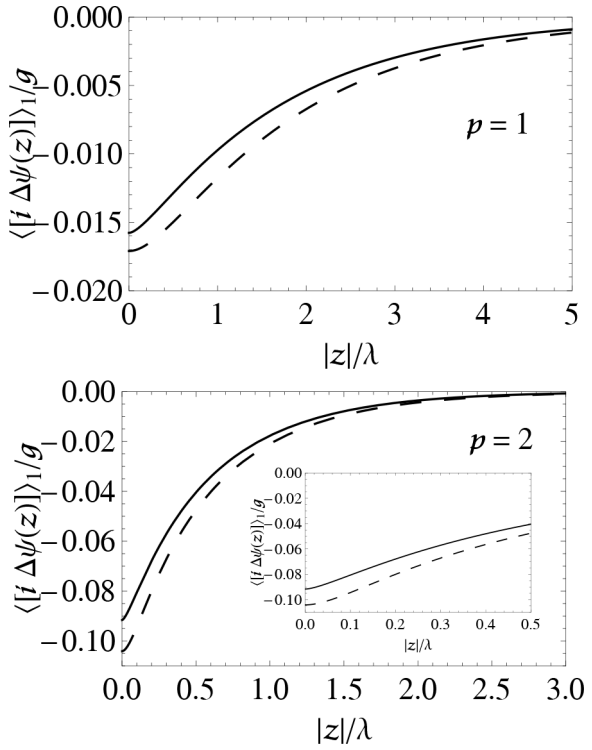

Fig. 18. A plot of the one-loop corrections to the electrostatic potential $\langle[\imath\Delta\psi(z)]\rangle_1$ (divided by g) as a function of z/λ, with $\tau = 0.6$, $\theta = 0.8$, and $s = 0.6$ for $p=1$ (top) and $p=2$ (bottom). For small $z/\lambda \ll 1$, $\langle[\imath\Delta\psi(z)]\rangle_1$ goes like z^2, so that $\partial_z\langle[\imath\Delta\psi(z)]\rangle_1|_{z=0} = 0$, as required by charge neutrality. (The bottom inset shows the behavior of $\langle[\imath\Delta\psi(z)]\rangle_1$ for $p=2$ as z approaches zero.) When $z/\lambda \gg 1$, $\langle[\imath\Delta\psi(z)]\rangle_1$ decays exponentially. The dashed line is $\langle[\imath\Delta\psi(z)]\rangle_1$ without charge regulation. Note that the overall magnitude of the $\langle[\imath\Delta\psi(z)]\rangle_1$ is smaller when there is charge regulation because the charge plate is partially neutralized.

something qualitatively different between monovalent and divalent counterions.

For short distances, we find

$$\langle[\imath\Delta\psi(z)]\rangle_1 = \langle[\imath\Delta\psi(0)]\rangle_1 + \mathcal{O}(z^2), \tag{A.24}$$

for both $p = 1$ and 2. Note that the fact that it goes like z^2 (see also fig. 18) is required by charge neutrality condition. The constant term is formally given by

$$\langle[\imath\Delta\psi(0)]\rangle_1 = \int \frac{\mathrm{d}^2\mathbf{q}}{(2\pi)^2}\frac{\ell_B}{\mathcal{W}(\alpha)}\left[\mathcal{H}_1(0) + \mathcal{M}(\alpha)\,\mathcal{H}_2(0)\right]. \tag{A.25}$$

An exact but long expression for $\langle[\imath\Delta\psi(0)]\rangle_1$ is presented in appendix B.

Appendix A.3. The grand potential and the Helmholtz free energy at one loop

In this subsection, we calculate the grand potential and Helmholtz free energy at one loop. The latter is needed to properly construct the phase diagrams in sect. 4. The grand potential, $\Omega[\phi]$, is defined by $\Omega[\phi] \equiv -k_BT \ln \mathcal{Z}_{\mu_\pm,\,\mu_{a\pm}}[\phi]$, where the grand partition function, $\mathcal{Z}_{\mu_\pm,\,\mu_{a\pm}}[\phi]$, is given by eq. (3). To one-loop order, we find

$$\begin{aligned}\beta\Omega_1[\phi] = \beta\Omega_0[\phi] &- \int \mathrm{d}^3\mathbf{x}\left[\frac{\delta\Lambda_{a+}}{\Lambda_{a+}^{(0)}}\,n_{a+} + \frac{\delta\Lambda_{a-}}{\Lambda_{a-}^{(0)}}\,n_{a-}\right]\delta(z)\\ &-\frac{\kappa^2}{(1+p)\ell_B}\int \mathrm{d}^3\mathbf{x}\left[\frac{\delta\Lambda_+}{p\Lambda_+^{(0)}}e^{p\varphi_0(z)} + \frac{\delta\Lambda_-}{\Lambda_-^{(0)}}e^{-\varphi_0(z)}\right]\\ &+\frac{1}{2}\ln\det\hat{\mathbf{K}} - \frac{1}{2}\ln\det\left[-\nabla_{\mathbf{x}}^2/\ell_B\right],\end{aligned} \tag{A.26}$$

where the first term on the right-hand-side is the mean-field grand potential, the next two terms come from the expansions of $\Lambda_{a\pm}$ and $\Lambda_\pm$, respectively (see eq. (8)), and the last two terms come from the "Gaussian" integration over the quadratic order of $\Delta\psi$ in eq. (8), and from the normalization constant, $\mathcal{N}_0$, in eq. (3), respectively.

At the mean-field level, the grand potential is simply given by the zero-loop action $\beta\Omega_0[\phi] = \mathcal{S}[\psi_0, \phi]$, which has the form $\beta\Omega_0[\phi] = -\wp\,\mathcal{V} + \Sigma_0\mathcal{A}$, as expected for an interfacial problem [55]. The pressure (in units of k_BT) is given by $\wp = \kappa^2/(p\ell_B) = (1+p)c_s$, from which we identify: $\kappa^2 = p(1+p)c_s\ell_B$, where c_s is the average salt concentration. The mean-field surface tension, Σ_0, is given by[6]

$$\begin{aligned}\Sigma_0 = \frac{n_0}{Z}\varphi_0(0) &- 2\left[n_{s+}^{(0)} + n_{s-}^{(0)}\right] - (n_{a+} + n_{a-})\\ &-\frac{n_0}{Z(1+p)}\ln\left[\frac{p\Lambda_+^{(0)}}{\Lambda_-^{(0)}}\right],\end{aligned} \tag{A.27}$$

[6] Note that there is an arbitrary constant U_0 in the external potential, $\phi(\mathbf{x})$. We have set $ZU_0 = (1+p)^{-1}\ln(p\Lambda_+^{(0)}/\Lambda_-^{(0)})$ in order to correctly produce the free energy for the counterion-only case in the limit $\Lambda_-^{(0)} \to 0$.

where we have defined

$$n_{s\pm}^{(0)} = \frac{\kappa^2}{(Z_\pm/Z)(1+p)\ell_B}\int_{-\infty}^{\infty}\mathrm{d}z\left[e^{\pm(Z_\pm/Z)\varphi_0(z)} - 1\right], \tag{A.28}$$

which may be interpreted as the mean-field Gibbs absorption of the positive and negative ions, respectively. The Gibbs adsorption has the following physical meanings: if it is positive, then particles tend to stay near the surface; if it is negative, the surface is depleted of particles. Next, the second and the third term in eq. (A.26) can be calculated, with the help of eqs. (24) and (26), to give a volume contribution

$$\beta\Delta\Omega_{2\mathrm{B}}/\mathcal{V} = -\frac{\kappa^2}{\ell_B}V_0 + \frac{\kappa^3}{8\pi}, \tag{A.29}$$

and a surface contribution

$$\begin{aligned}\beta\Delta\Omega_{2\mathrm{S}}/\mathcal{A} = &-\left(V_0 - \frac{\ell_B\kappa}{8\pi}\right)\left[p^2 n_{s+}^{(0)} + n_{s-}^{(0)}\right]\\ &-\left[V_0 - \frac{\ell_B\kappa}{8\pi} + \frac{1}{2}\,\mathcal{G}(0,0)\right]\left(p^2 n_{a+} + n_{a-}\right)\\ &+\left(p\,n_{a+} - n_{a-}\right)\langle[\imath\Delta\psi(0)]\rangle_1.\end{aligned} \tag{A.30}$$

Finally, the fundamental quantity to evaluate in eq. (A.26) is the functional determinant:

$$\beta\Delta\Omega \equiv \frac{1}{2}\ln\det\hat{\mathbf{K}} - \frac{1}{2}\ln\det\left[-\nabla_{\mathbf{x}}^2/\ell_B\right], \tag{A.31}$$

where $\hat{\mathbf{K}}$ is defined in eq. (14). Differentiating eq. (A.31) with respect to ℓ_B and using the identity: $\delta\ln\det\hat{\mathbf{X}} = \mathrm{Tr}\,\hat{\mathbf{X}}^{-1}\,\delta\hat{\mathbf{X}}$, for any operator $\hat{\mathbf{X}}$, we find

$$\begin{aligned}\frac{\partial\beta\Delta\Omega}{\partial\ell_B} = &\frac{1}{2\ell_B}\int \mathrm{d}^3\mathbf{x}\,G(\mathbf{x},\mathbf{x})\\ &\times\frac{\partial}{\partial\ell_B}\left\{\frac{\kappa^2}{1+p}\left[pe^{p\varphi_0(z)} + e^{-\varphi_0(z)}\right] + \frac{2}{\lambda_D}\delta(z)\right\},\end{aligned} \tag{A.32}$$

where we have made use of the fact that the inverse of $\hat{\mathbf{K}}$ in position space is the Green's function, $G(\mathbf{x},\mathbf{x}')$, and that the trace in position space corresponds to setting $\mathbf{x} = \mathbf{x}'$ and integrating over space. Writing $G(\mathbf{x},\mathbf{x})$ as a sum of 3 contributions: $G(\mathbf{x},\mathbf{x}) = 2V_0 - \ell_B\kappa/(4\pi) + \mathcal{G}(z,z)$, we see that eq. (A.32) has a volume and a surface contribution. The volume term can be written as

$$\frac{1}{\mathcal{V}}\frac{\partial\beta\Delta\Omega_{\mathrm{B}}}{\partial\ell_B} \equiv +\frac{1}{2\ell_B}\left(2V_0 - \frac{\kappa\ell_B}{4\pi}\right)\frac{\partial\kappa^2}{\partial\ell_B}, \tag{A.33}$$

which can be integrated back to give $\beta\Delta\Omega_{\mathrm{B}}$. The first term, which represents the bare self-energy term, precisely cancels the bare self-energy term in eq. (A.29). It is straightforward to show that the second term is simply the standard Debye-Huckel result for a homogeneous electrolyte: $\beta\Delta\Omega_{\mathrm{DH}}/\mathcal{V} = -\kappa^3/(12\pi)$ [51].

The surface contribution to eq. (A.32) contains four contributions. The first one is the self-energy terms that

cancel the bare self energies in eq. (A.30). The second term is the Debye-Huckel surface term

$$\beta\Delta\Omega_{\rm S2}/\mathcal{A} = -\frac{\kappa\ell_B}{8\pi}\left\{\left[p^2 n^{(0)}_{s+} + n^{(0)}_{s-}\right] + (p^2 n_{a+} + n_{a-})\right\}, \tag{A.34}$$

which cancels the corresponding terms in eq. (A.30). The third and fourth surface terms are

$$\begin{aligned}\frac{\partial\beta\Delta\omega_{\rm 3d}}{\partial\ell_B} \equiv \frac{1}{\mathcal{A}}\frac{\partial\beta\Delta\Omega_{\rm S3}}{\partial\ell_B} &\equiv \frac{1}{2\ell_B}\int_{-\infty}^{\infty}{\rm d}z\,\mathcal{G}(z,z)\\ &\times\frac{\partial}{\partial\ell_B}\left\{\frac{\kappa^2}{1+p}\left[p\,e^{p\varphi_0(z)} + e^{-\varphi_0(z)}\right]\right\}\\ &-\ell_B\left[p^2 n^{(0)}_{s+} + n^{(0)}_{s-}\right]\frac{\partial}{\partial\ell_B}\left(\frac{V_0}{\ell_B} - \frac{\kappa}{8\pi}\right), \end{aligned}\tag{A.35}$$

$$\begin{aligned}\frac{\partial\beta\Delta\omega_{\rm 2d}}{\partial\ell_B} \equiv \frac{1}{\mathcal{A}}\frac{\partial\beta\Delta\Omega_{\rm S4}}{\partial\ell_B} &\equiv \frac{1}{2\ell_B}\,\mathcal{G}(0,0)\,\frac{\partial}{\partial\ell_B}\left(\frac{2}{\lambda_D}\right)\\ &-\ell_B\left(p^2 n_{a+} + n_{a-}\right)\frac{\partial}{\partial\ell_B}\left(\frac{V_0}{\ell_B} - \frac{\kappa}{8\pi}\right). \end{aligned}\tag{A.36}$$

Integrating eqs. (A.35) and (A.36) with respect to ℓ_B, and after some algebra, we find that the sum, $\beta\Delta\omega_{\rm 2d} + \beta\Delta\omega_{\rm 3d}$, can be written as

$$\begin{aligned}\beta\Delta\omega_{\rm 2d} + \beta\Delta\omega_{\rm 3d} \equiv \frac{1}{2}\int\frac{{\rm d}^2\mathbf{q}}{(2\pi)^2}\Bigg\{&-2\ln\Phi_i(\alpha)\\ &+\ln\left[\frac{-h'_-(0)h_-(0)}{\alpha\kappa} + \frac{h^2_-(0)}{\alpha\kappa\lambda_D}\right]\\ &-\frac{\ell_B}{2\alpha\kappa}\left[p^2 n^{(0)}_{s+} + n^{(0)}_{s-} + p^2 n_{a+} + n_{a-}\right]\Bigg\}, \end{aligned}\tag{A.37}$$

where $\Phi_1(\alpha) = 1 + 1/\alpha$ and $\Phi_2(\alpha) = (1+1/\alpha)[1+1/(2\alpha)]$ for $p = 1$ and $p = 2$, respectively, and $h_-(0)$ is one of the homogeneous solutions given by eq. (A.6) evaluated at $z = 0$.

We are now in a position to obtain explicit expressions for the grand potential and the Helmholtz free energy for our system. The grand potential can be expressed as $\beta\Omega_1[\phi] = -\wp_1\mathcal{V} + \Sigma_1\mathcal{A}$. The bulk pressure at one-loop, $\wp_1$, has three contributions: a mean-field contribution, $\wp = \kappa^2/(p\ell_B) = (1+p)c_s$, a contribution coming from the second term in eq. (A.29), and a contribution coming from the functional determinant, eq. (A.33). Therefore, $\wp_1 = (1+p)c_s - \kappa^3/(8\pi) + \kappa^3/(12\pi) = (1+p)c_s - \kappa^3/(24\pi)$, which is precisely the pressure for a homogeneous electrolyte. Similarly, the surface tension to one loop is

$$\begin{aligned}\Sigma_1 = \Sigma_0 &+ (pn_{a+} - n_{a-})\,\langle[\imath\Delta\psi(0)]\rangle_1\\ &-\frac{1}{2}\,\mathcal{G}(0,0)\left(p^2 n_{a+} + n_{a-}\right) + \beta\Delta\omega_{\rm 2d} + \beta\Delta\omega_{\rm 3d}. \end{aligned}\tag{A.38}$$

The Helmholtz free energy at the one-loop level is related to the grand-canonical potential by

$$\begin{aligned}\beta F_1 = \beta\Omega_1[\phi] &+ \sum_{i=\pm}\mu_i^{(1)}\int{\rm d}^3\mathbf{x}\,\langle\hat{\rho}_i(\mathbf{x})\rangle_1\\ &+\sum_{i=\pm}\mu_{ai}^{(1)}\int{\rm d}^3\mathbf{x}\,\langle\hat{\rho}_{ai}(\mathbf{x})\rangle_1, \end{aligned}\tag{A.39}$$

with the one-loop ion distributions given by eqs. (22) and (23). The chemical potentials to one loop are given by

$$\mu_\pm^{(1)} = \ln\left(\frac{\Lambda_\pm^{(0)} a_\pm^3}{\ell_B}\right) - (Z_\pm/Z)^2\,\left(\frac{\ell_B\kappa}{8\pi}\right), \tag{A.40}$$

$$\begin{aligned}\mu_{a\pm}^{(1)} = \ln\left(\frac{\Lambda_{a\pm}^{(0)} a_{c\pm}^2}{\ell_B}\right) &\mp (Z_\pm/Z)\langle[\imath\Delta\psi(0)]\rangle_1\\ &-(Z_\pm/Z)^2\,\left(\frac{\ell_B\kappa}{8\pi}\right) + \frac{1}{2}\,(Z_\pm/Z)^2\,\mathcal{G}(0,0). \end{aligned}\tag{A.41}$$

The free energy has the form: $F_1 = f_{\rm B}^{(1)}\,\mathcal{V} + f_{\rm S}^{(1)}\mathcal{A}$. We find that the bulk contribution to the free energy is precisely the Debye-Huckel free energy:

$$\begin{aligned}\beta f_{\rm B}^{(1)} &= -\wp_1 - \frac{\kappa^3}{8\pi} + \frac{\kappa^2}{p\ell_B}\ln\left[\frac{\kappa^2 a^3}{p(1+p)\ell_B}\right]\\ &= (1+p)\,c_s\left[\ln\left(c_s a^3\right) - 1\right] - \frac{\kappa^3}{12\pi}, \end{aligned}\tag{A.42}$$

where $a \equiv (p^{p/3}\,a_+\,a_-^p)^{1/(1+p)}$. The surface contribution is given by

$$\begin{aligned}\beta f_{\rm S}^{(1)} = &\sum_{i=\pm} n_{ai}\left[\ln\left(n_{ai}\,a_{ci}^2\,e^{-\varepsilon_i}\right) - 1\right]\\ &-\frac{\kappa\ell_B}{8\pi}(p^2 n_{a+} + n_{a-}) + \beta\Delta\omega_{2d}\\ &+n_{s+}\ln\left[\frac{\kappa^2\,a_+^3}{p(1+p)\ell_B}\right] + n_{s-}\ln\left[\frac{\kappa^2\,a_-^3}{(1+p)\ell_B}\right]\\ &-2\left[n^{(0)}_{s+} + n^{(0)}_{s-}\right] + (pn_{s+} - n_{s-})\,\varphi_0(0)\\ &-\frac{\kappa\ell_B}{8\pi}\left[p^2 n^{(0)}_{s+} + n^{(0)}_{s-}\right] + \beta\Delta\omega_{3d}, \end{aligned}\tag{A.43}$$

where $\beta\Delta\omega_{\rm 2d} + \beta\Delta\omega_{\rm 3d}$ is given by eq. (A.37), $n_{s\pm} \equiv n_\pm^{(0)} + \Delta n_{s\pm}$, are the one-loop Gibbs adsorption of the positive and negative ions, respectively, and the one-loop corrections terms $\Delta n_{s\pm}$ are given by

$$\begin{aligned}\Delta n_{s\pm} \equiv &\frac{\kappa^2}{(Z_\pm/Z)(1+p)\ell_B}\int_{-\infty}^{+\infty}{\rm d}z\,e^{\pm(Z_\pm/Z)\varphi_0(z)}\\ &\times\left[\pm(Z_\pm/Z)\langle[\imath\Delta\psi(z)]\rangle_1 - \frac{1}{2}(Z_\pm/Z)^2\mathcal{G}(z,z)\right]. \end{aligned}\tag{A.44}$$

In eq. (A.43), we have discarded a term that is higher order in ℓ_B, namely, $\propto \kappa\ell_B\Delta n_{s\pm}$. Note that the expression for the surface free energy at one loop given by eq. (A.43) is general, valid for arbitrary p. The first three terms in $\beta f_{\rm S}^{(1)}$ represent the free energy (one loop) of the adsorbed ions, and the rest of terms represent the free energy of the ions in the bulk. It should also be mentioned that eq. (A.43) also contain a logarithmic divergent term associated with the free energy of charge fluctuations in 2d represented by $\omega_{\rm 2d}$ [45] (see footnote[5]). We close this section by pointing

$$\mathcal{M}(\alpha)=\begin{cases}\dfrac{\nu+2\theta(\nu^2-\alpha^2 s^2)}{(\alpha s+\nu)[(1-\tau)^2+(\alpha s+2\theta)(\alpha s+\nu)]}\,, & \text{for } p=1,\\ -\dfrac{c_0(a_0-a_2\alpha^2)}{b_0(b_0+b_1\alpha+b_2\alpha^2)(c_0+c_1\alpha+c_2\alpha^2+c_3\alpha^3)}-\dfrac{\alpha(\alpha^2-1)(4\alpha^2-1)(1+\gamma_2)^4(1-4\gamma_2+\gamma_2^2)^4}{(e_0+e_1\alpha+e_2\alpha^2+e_3\alpha^3)(c_0+c_1\alpha+c_2\alpha^2+c_3\alpha^3)}\,, & \text{for } p=2,\end{cases} \tag{A.2}$$

$$\mathcal{G}_{3d}(0,0)=\begin{cases}-\dfrac{\ell_B}{4\pi\lambda}\left\{\theta\ln\left[\dfrac{(s+2\theta)^2}{(\nu+2\theta)(s+\nu)}\right]+2\left[(1-\tau)^2+\nu\theta-2\theta^2\right]\left|\dfrac{\tanh^{-1}\left(\frac{\sqrt{(\nu-2\theta)^2-4(1-\tau)^2}}{2s+\nu+2\theta}\right)}{\sqrt{(\nu-2\theta)^2-4(1-\tau)^2}}\right|\right\}, & \text{for } p=1,\\ -\dfrac{\kappa\ell_B}{4\pi}\displaystyle\int_1^\infty \mathrm{d}\alpha\frac{\alpha(\kappa\lambda_D)^2(c_0+6\alpha\gamma_2 d_0)}{(1+\alpha\kappa\lambda_D)(e_0+e_1\alpha+e_2\alpha^2+e_3\alpha^3)}, & \text{for } p=2.\end{cases} \tag{A.3}$$

$$\mathcal{B}_1(\alpha)=\frac{1}{8\alpha^4}\begin{cases}\alpha^2\dfrac{2(1-\tau)^2+s^2}{s\sqrt{s^2+(1-\tau)^2}}\,, & \text{for } p=1,\\ \dfrac{(1-\gamma_2^2)}{(1-4\gamma_2+\gamma_2^2)d_3}\left\{\alpha^2\left[5d_3+12\gamma_2\left(1-\gamma_2+\gamma_2^2\right)\right]-\left[5d_3+6\gamma_2\left(1-\gamma_2\right)^2\right]\right\}, & \text{for } p=2,\end{cases} \tag{A.4}$$

out that the equilibrium values for $n_{a\pm}$ as given eq. (32) can be obtained by minimizing $f_{\rm S}^{(1)}$ with respect to $n_{a\pm}$, as they should be.

Appendix B. Long mathematical expressions

In this appendix, we present those long mathematical expressions that might have been too distracting to be put in the main text. First, we give an exact solution for γ_2, and then we list the long expressions for $\mathcal{M}(\alpha)$, $\mathcal{G}_{3d}(0,0)$, $\mathcal{B}_i(q)$, and $\langle[i\Delta\psi(0)]\rangle_1$.

Equation (36) can be recast into a cubic equation, which can actually be solved. The solution γ_2 can be written as

$$\gamma_2=1-\frac{s}{1-\tau}+\frac{2}{|1-\tau|}\cos(\Theta/3), \tag{B.1}$$

where $s\equiv\kappa\lambda$,

$$\Theta\equiv\begin{cases}2\pi-\tan^{-1}|A/B|\,, & \text{for } \tau<1 \text{ and } B<0,\\ \pi+\tan^{-1}|A/B|\,, & \text{for } \tau<1 \text{ and } B>0,\\ 2\pi+\tan^{-1}|A/B|\,, & \text{for } \tau>1,\end{cases}$$

with

$$A\equiv(1-\tau)\sqrt{3\,s^4+12(1-\tau)^2s^2+16(1-\tau)^4},$$
$$B\equiv 4\,(1-\tau)^3-6(1-\tau)^2 s+3(1-\tau)s^2-2s^3.$$

The expression for $\mathcal{M}(\alpha)$ is formally given by eq. (A.5), valid for $p=1$ and $p=2$. Explicitly, we find

see eq. (A.2) *above*

where $\theta\equiv Z(n_{a+}+n_{a-})/n_0$, $\nu\equiv\sqrt{s^2+(1-\tau)^2}$, $s\equiv\kappa\lambda$, $a_0\equiv(1+\gamma_2)^6$, $a_2\equiv(1+\gamma_2)^4(1+8\gamma_2+\gamma_2^2)-36\gamma_2^2(1+\gamma_2^2)$, $b_0\equiv(1+\gamma_2)^3$, $b_1\equiv3(1-\gamma_2)(1+\gamma_2^2)$, $b_2\equiv2(1+\gamma_2)(1-4\gamma_2+\gamma_2^2)$, $c_0\equiv6\gamma_2(1-\gamma_2)(1+\gamma_2)^3$, $c_1\equiv(1+\gamma_2)^6-72\gamma_2^3$, $c_2\equiv b_1b_2/2=3(1-4\gamma_2+\gamma_2^2-\gamma_2^4+4\gamma_2^5-\gamma_2^6)$, $c_3\equiv b_2^2/2=2(1-6\gamma_2+3\gamma_2^2+20\gamma_2^3+3\gamma_2^4-6\gamma_2^5+\gamma_2^6)$, $e_0\equiv c_0\kappa\lambda_D+b_0b_2/2$, $e_1\equiv c_2+c_1\kappa\lambda_D$, $e_2\equiv c_3+c_2\kappa\lambda_D$, and $e_3\equiv c_3\kappa\lambda_D$. As one can probably surmise, the calculation for $p=2$ is extremely complicated.

The expression for $\mathcal{G}_{3d}(0,0)$ is formally given by eq. (A.13), which is valid for $p=1$ and 2. Explicitly, we find

see eq. (A.3) *above*

The expression for $\mathcal{B}_i(\alpha)$ is formally given by eq. (A.17). Explicitly, we find

see eq. (A.4) *above*

and

see eq. (B.5) *on the next page*

The expression for $\langle[i\Delta\psi(0)]\rangle_1$ is formally given by eq. (A.25). Explicitly, we find

see eq. (B.6) *above*

where $d_0\equiv1+4\gamma_2-6\gamma_2^2+4\gamma_2^3+\gamma_2^4$, $d_1\equiv(1-\gamma_2)a_2=1+11\gamma_2-9\gamma_2^2+53\gamma_2^3-53\gamma_2^4+9\gamma_2^5-11\gamma_2^6-\gamma_2^7$, $d_2\equiv b_0b_2/2-6\gamma_2d_0=1-6\gamma_2-33\gamma_2^2+20\gamma_2^3-33\gamma_2^4-6\gamma_2^5+\gamma_2^6$, $d_3\equiv1-2\gamma_2+6\gamma_2^2-2\gamma_2^3+\gamma_2^4$.

$$\mathcal{B}_2(\alpha) = \begin{cases} -\dfrac{(1-\tau)^2+2\alpha^2}{8\alpha^3} - \dfrac{2(1-\tau)^2+3s^2}{8\alpha^2 s\sqrt{1+s^2}}\,, & \text{for } p=1, \\ -\dfrac{3[(1-\gamma_2^2)+2\alpha(1+\gamma_2^2)]}{2\gamma_2(4\alpha^2-1)} + \dfrac{1}{\alpha}\left[\dfrac{17-14\gamma_2+17\gamma_2^2}{24\gamma_2} - \dfrac{\gamma_2(1-\gamma_2+\gamma_2^2)}{d_3}\right] \\ +\dfrac{(1-\gamma_2^2)}{4\alpha^2}\left[\dfrac{2d_3-9\gamma_2(1+4\gamma_2+\gamma_2^2)}{\gamma_2(1+\gamma_2)b_2} - \dfrac{(2+\gamma_2+2\gamma_2^2)}{d_3}\right] \\ +\dfrac{\gamma_2(1+\gamma_2)}{4\alpha^3}\left[\dfrac{d_3-6\gamma_2(7-2\gamma_2+7\gamma_2^2)}{3b_2\gamma_2^2} - \dfrac{b_2}{d_3(1+\gamma_2)^2}\right] - \dfrac{3(1-\gamma_2^2)}{4\alpha^4(1-4\gamma_2+\gamma_2^2)} - \dfrac{1}{8\alpha^5}\,, & \text{for } p=2. \end{cases} \tag{B.5}$$

$$\langle [i\Delta\psi(0)] \rangle_1 = \begin{cases} -\dfrac{\ell_B(1-\tau)}{16\pi\lambda}\left[\dfrac{1}{2}\ln\left(\dfrac{2\theta+\nu}{s+\nu}\right) + \left[\frac{2}{\nu}(1-\tau)^2+\nu+6\theta\right]\left|\dfrac{\tanh^{-1}\left(\frac{\sqrt{(\nu-2\theta)^2-4(1-\tau)^2}}{2s+\nu+2\theta}\right)}{\sqrt{(\nu-2\theta)^2-4(1-\tau)^2}}\right|\right], & \text{for } p=1, \\ -\dfrac{\ell_B\kappa}{32\pi}\displaystyle\int_1^\infty \frac{d\alpha}{d_3}\left[\frac{b_0d_0+d_1\alpha}{b_0+b_1\alpha+b_2\alpha^2} + \frac{2d_0e_0+(b_2d_1-2d_0d_2\kappa\lambda_D)\,\alpha - b_2d_1\kappa\lambda_D\alpha^2}{2(e_0+e_1\alpha+e_2\alpha^2+e_3\alpha^3)}\right], & \text{for } p=2, \end{cases} \tag{B.6}$$

References

1. J.N. Israelachvili, *Intermolecular and Surface Forces* (Academic Press Inc., San Diego, 1992).
2. S. Durand-Vidal, J.P. Simonin, D. Turq, *Electrolytes at Interfaces* (Kluwer, Dordrecht, 2000).
3. D. Andelman, in *Handbook of Biological Physics*, Vol. **1**, edited by R. Lipowsky, E. Sackmann (Elsevier, Amsterdam, 1995) Chapt. 12.
4. Yan Levin, Rep. Prog. Phys. **65**, 1577 (2002).
5. P. Attard, J. Phys. Chem. **99**, 14174 (1995).
6. A.G. Moreira, Roland R. Netz, in *Electrostatic Effects in Soft Matter and Biophysics*, edited by C. Holm, P. Kekicheff, R. Podgornik (Kluwer, Boston, 2001).
7. A.Y. Grosberg, T.T. Nguyen, B.I. Shklovskii, Rev. Mod. Phys. **74**, 329 (2002).
8. A.W.C. Lau, Phys. Rev. E **77**, 011502 (2008).
9. T. Markovich, D. Andelman, R. Podgornick, EPL **106**, 16002 (2014).
10. T. Markovich, D. Andelman, R. Podgornick, J. Chem. Phys. **142**, 044702 (2015).
11. T. Markovich, D. Andelman, R. Podgornick, Langmuir **33**, 34 (2017).
12. T. Markovich, D. Andelman, H. Orland, J. Chem. Phys. **145**, 134704 (2016).
13. R. Messina, J. Phys.: Condens. Matter **21**, 113102 (2009).
14. L. Guldbrand, B. Jönsson, H. Wennerström, P. Linse, J. Chem. Phys. **80**, 2221 (1984).
15. G.M. Kepler, S. Fraden, Phys. Rev. Lett. **73**, 356 (1994).
16. J.C. Butler, T. Angelini, J.X. Tang, G.C.L. Wong, Phys. Rev. Lett. **91**, 028301 (2003).
17. D. Grier, Y. Han, J. Phys.: Condens. Matter **16**, S4145 (2004).
18. A.R. Saito, M.C. Parez, J.S. Solano, J.L.A. Lara, Phys. Rev. E **67**, 050403 (2003).
19. R.M. Pashley, J. Colloid Interf. Sci. **83**, 531 (1981).
20. P. Sinha, I. Szilagyi, F. Javier, M.R. Cabello, P. Maroni, M. Borkovec, J. Phys. Chem. **4**, 648 (2013).
21. F.J. Montes, M.R. Cabello, G. Trefalt, P. Maroni, M. Borkovec, Langmuir **30**, 4451 (2014).
22. I. Popa, P. Sinha, M. Finessi, P. Maroni, G. Papastavrou, M. Borkovec, Phys. Rev. Lett. **104**, 228301 (2010).
23. D. Ebeling, D. Ende, F. Mugele, Nanotechnology **22**, 305706 (2011).
24. M. Dishon, O. Zohar, U. Sivan, Langmuir **25**, 2831 (2009).
25. G.L. Gouy, J. Phys. Radium **9**, 457 (1910).
26. D. Champan, Philos. Mag. Sixth Ser. **25**, 475 (1913).
27. B.W. Ninham, V.A. Parsegian, J. Theor. Biol. **31**, 405 (1971).
28. D.Y.C. Chan, T.W. Healy, L.R. White, J. Chem. Soc., Faraday Trans. I **72**, 2844 (1976).
29. N. Boon, R. Roij, J. Chem. Phys. **134**, 054706 (2011).
30. R. Podgornik, J. Chem. Phys. **149**, 104701 (2018).
31. J. Lyklema, Pure Appl. Chem. **63**, 895 (1991).
32. See, for example, M.C. Desjonqueres, D. Spanjaard, *Concepts in Surface Physics*, 2nd edition (Springer, New York, 1996).
33. D. Harries, R. Podgornik, V.A. Parsegian, E. May-Or, D. Andelman, J. Chem. Phys. **124**, 224702 (2006).
34. A. Majee, M. Bier, R. Podgornik, Soft Matter **14**, 985 (2018).
35. A. Majee, M. Bier, R. Blossey, R. Podgornik, Phys. Rev. E **100**, 050601(R) (2019).
36. N. Adzic, R. Podgornik, Eur. Phys. J. E **37**, 49 (2014).
37. N. Adzic, R. Podgornik, J. Chem. Phys. **144**, 214901 (2016).
38. N. Adzic, R. Podgornik, Phys. Rev. E **91**, 022715 (2015).
39. I. Langmuir, J. Am. Chem. Soc. **38**, 2221 (1916).
40. I. Langmuir, J. Am. Chem. Soc. **40**, 1361 (1918).
41. R.H. Fowler, E.A. Guggenheim, *Statistical Thermodynamics* (University Press, Cambridge, 1939).
42. B.S. Lu, X. Xing, Phys. Rev. E **89**, 032305 (2014).
43. J. Hubbard, Phys. Rev. Lett. **3**, 77 (1959).
44. R.L. Stratonovitch, Dokl. Akad. Nauk USSR **115**, 1907 (1957).
45. See, for example, A.W.C. Lau, PhD Thesis, University of California, Santa Barbara (2000).
46. D.C. Grahame, J. Chem. Phys. **21**, 1054 (1953).
47. Luc Belloni, Colloids Surf. A **140**, 227 (1998).
48. A.W.C. Lau, D.B. Lukatsky, P. Pincus, S.A. Safran, Phys. Rev. E **65**, 051502 (2002).
49. A. Thomy, X. Duval, J. Regnier, Surf. Sci. Rep. **1**, 1 (1981).
50. R.H. Fowler, Proc. Camb. Philos. Soc. **32**, 144 (1935).
51. L.D. Landau, E.M. Lifshitz, *Statistical Physics*, 3rd ed. (Pergamon, New York, 1980).

52. J.W. Evans, Rev. Mod. Phys. **65**, 1281 (1993).
53. K.V. Tretiakov, K.J.M. Bishop, B. Kowalczyk, A. Jaiswal, M.A. Poggi, B.A. Grzybowski, J. Phys. Chem. A **113**, 3799 (2009).
54. Joseph Lajzerowicz, Jean Sivardiere, Phys. Rev. A **11**, 2019 (1975).
55. R. Evans, Adv. Phys. **28**, 143 (1979).